Paper accepted by Journal of Sound and Vibration, 1 November 2020

Combining the 2.5D FE-BE method and the TMM method to study the vibro-acoustics of acoustically treated rib-stiffened panels

Tiesong Deng [a], Muxiao Li [a], Shumin Zhang [a], Xiaozhen Sheng [b*], David J. Thompson [c]

[a] *State Key Laboratory of Traction Power, Southwest Jiaotong University, Chengdu, China*

[b] *School of Urban Railway Transportation, Shanghai University of Engineering Science, Shanghai, China*

[c] *Institute of Sound and Vibration Research, University of Southampton, Southampton, UK*

[*] *Correponding author. E-mail address: shengxiaozhen@hotmail.com*

Abstract

This paper is concerned with the prediction of the vibro-acoustic behaviour of rib-stiffened panels treated with multiple layers of porous materials. The acoustically treated rib-stiffened panels are assumed to be uniform and infinitely long in one direction (the longitudinal direction) but the cross-section can have an arbitrary and often complicated shape. Although the two-and-half dimensional structural finite element method (2.5D FEM) and the two-and-half dimensional acoustic boundary element method (2.5D BEM) may be combined to perform the vibro-acoustic prediction, the presence of the multiple layers of acoustic treatment often makes the prediction too time-consuming. More efficient methods are required for such structures and the aim of this paper is to propose such a method. The rib-stiffened panel and the fluid domain containing the incident and reflected sound waves are modelled using 2.5D FEM-BEM while the acoustic treatment layer and the fluid domain containing the transmitted sound waves are dealt with, approximately, using the transfer matrix method (TMM). The coupling of TMM and 2.5D FEM-BEM is formulated in detail. Since the acoustically treated panel is assumed to be flat and baffled, the 2.5D BEM is based on the Rayleigh integral in the wavenumber domain. Meanwhile, the TMM is based on a two-dimensional Fourier transform which implies that the porous layers also extend to cover the baffle; the validity of this assumption is explored. The accuracy and efficiency of the method is compared with a full 2.5D FE-BE method for a homogeneous plate with attached layers of absorbent material. It is shown that the method proposed in this paper can reduce calculation time by about a factor of three compared with the full 2.5D FE-BE method. The proposed method is then applied to study the sound transmission loss (STL) of a typical rib-stiffened panel from a train carriage which is acoustically treated with different porous material layers, demonstrating that the design of the

acoustic treatment can have a significant effect on the STL of the panel.

Keywords: Rib-stiffened panels; Acoustic treatment layer; Sound transmission; 2.5D finite-boundary element method; Transfer matrix method

1. Introduction

1.1 Review of related literatures

Rib-stiffened panels are structures which are widely used in engineering, such as in railway vehicles [1], marine vessels [2] and aircraft [3], due to their light weight, high static stiffness and strength. With increasing emphasis on the comfort of on-board staff and passengers, these panels are also required to have high vibro-acoustic performance. A bare rib-stiffened panel often has poorer vibro-acoustic performance than the mass law of the equivalent simple panel [4, 5], especially at high frequencies due to the presence of many local modes. To overcome this, acoustic treatments are often applied to the panel. These can be layers of sound absorbing material on the interior surface [6], free or constrained damping layers on the exterior surface [7], or filling of voids in the panel with damping or absorbing materials [8]. The design of a rib-stiffened panel and the application of acoustic treatment require predictions of the vibro-acoustic behaviour of the panel. However, the complex geometry of the rib-stiffened panel often makes the prediction a difficult task, and with the acoustic treatment the task becomes even more difficult and very time-consuming.

The vibro-acoustic behaviour of rib-stiffened panels, including wave propagation, sound radiation and sound transmission loss (STL), has previously been investigated using different methods. Analytical methods have been used for simple rib-stiffened panels. For example, by treating the ribs as equivalent beams or spring-mass-spring systems, Lee et al. [9, 10] investigated the STL of a single-leaf rib-stiffened panel and Wang et al. [11] investigated that of a double-leaf one. In these studies, the ribs are periodically arranged and the spatially harmonic approach making use of the periodicity is employed to derive the structural and acoustic responses. However, for panels with a complex-sectional geometry or irregularly distributed ribs, such analytical approaches cannot be used.

Analytical approaches can also be used to deal with simple structures with acoustic treatment. In Ref. [12], to determine the STL of a rectangular plate laminated with a porous layer, a normal surface impedance is used to replace the porous layer. The model in Ref. [12] assumes the porous layer to be acoustically locally reacting and use is made of the normal surface impedance measured

with a fixed back surface (as in an impedance tube); the bending vibration of the skeleton and the interaction between the porous material layer and the back plate are all neglected. This approach may cause significant errors in STL prediction if the porous material layer is not sufficiently light, thin and soft. For a sandwich composite formed of doubly curved face sheets, the influences of embedded poro-elastic cores and boundary conditions on STL are investigated in Refs. [13, 14]. More applications of analytical approaches can be found in Refs. [6, 8, 15, 16].

The conventional finite element method (FEM) is commonly used for complex structures [17]. To produce reasonably accurate results, at least six nodes are required for each wavelength, often resulting in very large computation costs at high frequencies. Therefore, at high frequencies, alternative methods are often applied. For example, Xie et al., after working out the mode count and modal density of an extruded aluminium panel used in railway vehicles [18], investigated its sound radiation and STL using statistical energy analysis (SEA) [4]. In SEA, a structure is divided into a number of subsystems, such as beams, plates or simple rib-stiffened panels. It is required that the subsystems are coupled weakly and that there is a sufficient number of resonant modes in a frequency band in each subsystem [19]. If these requirements are not satisfied, SEA may be inapplicable. For example, in some structures, modes with long wavelengths and those with short wavelengths may co-exist in the so-called mid-frequency range, for which the SEA requirements on the number of modes are only partially met. To address this, a hybrid FE/SEA method was developed by Langley et al. [20] for the mid-frequency vibro-acoustics of complex structures. By applying the method to a framework-panel structure, the method was validated numerically in Ref. [21] and experimentally in Ref. [22]. According to this hybrid method, the system degrees of freedom are divided into a long wavelength part and a short wavelength part. The former is described by FEM and the latter by SEA and a coupling is defined between them in terms of power transmission between them.

Engineering structures are often designed and constructed with some degree of periodicity. Uniformity in one direction is a special case of periodicity in that direction. For such structures, a method termed wave-based finite element method [23, 24], also known as the periodic unit cell method (PUC) [25], can be used. Recently, this method was extended by Errico et al. to study the vibrations and sound transmission of flat, curved and axisymmetric structures under both uncorrelated (diffuse field acoustic) and spatially-correlated (turbulent boundary layer) loads [26, 27]. The extension was made by introducing an approximate excitation model to reproduce the

uncorrelated and spatially-correlated loads using a wavenumber integration of surface waves [27]. This method has also been used to determine SEA parameters for complex vibro-acoustic systems [28]. It is established from the periodic structure theory, in which a representative unit cell is selected and analysed under periodic boundary conditions to produce propagation properties (e.g. propagation constant, group velocity etc.) for a periodic structure formed of the unit cell. These propagation properties can be used to determine the vibro-acoustic behaviour of the entire periodic structure or the SEA parameters of the unit cell. With such an approach, Chronopoulos et al. [29] predicted the radiation efficiency and STL of a sandwich panel. Orrenius et al. [25] gave a literature review on wave-based modelling methods in predictive vibro-acoustics, and compared the PUC method with the 2.5D FEM by applying these two methods to a complex rib-stiffened panel. They concluded that the 2.5D FEM is more convenient than the PUC for producing dispersion relations, since the dispersion equation of the 2.5D FE model can be converted to a standard eigenvalue problem while that of the PUC model is a generalized and nonlinear eigenvalue problem, requiring a sophisticated zero-point searching algorithm.

The 2.5D FEM, also known as the waveguide finite element method, is particularly suitable for a structure that is uniform and effectively infinite in one direction (termed the longitudinal direction). The rib-stiffened panels used in train carriages may be idealised as such a structure. Since the structure is considered to be infinitely long, its dynamic response can be expressed as the superposition of structural waves propagating in the longitudinal direction at particular wavenumbers. Since the cross-section of the structure is uniform in the longitudinal direction, each wave can be solved independently based on a 2D FE mesh of the cross-section, although responses in all three directions are predicted. This gives the method the name of 2.5D FEM. The method has been used to study wave propagation characteristics in rib-stiffened panels [30] and railway track systems [31, 32].

To calculate the acoustic field, the boundary element method (BEM) is normally used. When the acoustic boundary is infinitely long and the boundary conditions are uniform in that direction, the acoustic field can also be expressed as the superposition of sound waves propagating in the longitudinal direction at particular wavenumbers. This is the basis of the 2.5D BEM. The 2.5D FEM and 2.5D BEM can be coupled to investigate the vibro-acoustics of long and uniform structures. Prasetiyo [33] used this method to study the vibro-acoustic behaviour of an infinitely long plate and compared it with an analytical model, showing a good agreement. Nilsson et al. [7] predicted, using

the 2.5D FE-BE method, the STL of a complex extruded panel laminated with a rubber damping layer. They also measured the STL of the panel and found good agreement between prediction and measurement at high frequencies. With measured damping on a typical truss-core extruded panel, Zhang et al. [5] conducted a parametric study on the STL of the panel using the 2.5D FE-BE method. Due to the finite length of the panel in the longitudinal direction, the 2.5D FE-BE prediction deviates from measured values at low frequencies. Ref. [5] shows that the 2.5D FEM-BEM gives reasonable results for the STL when the acoustic wavelength in the longitudinal direction is shorter than half the length of the panel. To make the method applicable at low frequencies, a spatial window technique [34] was applied to the panel as well as the acoustic domains. This treatment was further applied to investigate the sound radiation from the panel due to excitation by a point force [35]. It is demonstrated in Refs. [34, 35] that improved agreement with measurement can be achieved at low frequencies with the spatial window technique.

When the full-space Green's functions are used in 2.5D BEM [33], the integral boundary is required to be closed. When evaluating the STL of a panel, it is usually treated as being mounted in an infinite baffle [36]; if the infinite baffle is represented using BEs, it has to be truncated, introducing errors to the STL prediction. This problem may be overcome by using the half-space Green's functions [37]. However, the complexity of the half-space Green's functions will increase the computation cost. Fortunately, the panel can often be considered to be coplanar with the baffle and the half-space boundary integral reduces to the classic Rayleigh integral. When the panel is infinitely long, the Rayleigh integral can also be transformed into the wavenumber domain [38], which, when combined with the 2.5D FEM, is ideally suited to the vibro-acoustic analysis of a panel which is uniform and infinitely long in the longitudinal direction. In this method, the boundary elements are only needed on the surface of the panel. In the current paper, as in Ref. [38], the wavenumber domain Rayleigh integral will be applied in the 2.5D BEM and coupled with the 2.5D FEM to study the vibro-acoustics of rib-stiffened panels which are uniform and unbounded in the longitudinal direction.

In practice, a rib-stiffened panel is normally combined with other structures or materials for a number of purposes, such as heat insulation, vibration control, sound insulation or absorption. In train carriages, the panels are usually acoustically treated by applying multiple layers of porous material on their inward-facing surface, above which the floor structure or interior trim is placed. However, the aforementioned 2.5D method cannot be directly applied to evaluate the STL due to

the presence of the porous material layers. The porous material may be regarded as an equivalent fluid having frequency-dependent density and bulk modulus. These parameters may be determined either using empirical models [39, 40] or using rigid-frame models [41, 42]. In the empirical and rigid-frame models, the mass of the porous material and the vibration of the skeleton are not considered. With increasing computation capacity, Biot's theory [43, 44] for the propagation of elastic waves in a fluid-saturated porous medium is gaining more and more attentions.

For the vibro-acoustic behaviour of an unbounded layered structure consisting of homogeneous material layers, air layers or porous material layers, the computationally-efficient transfer matrix method (TMM) is normally used [45]. However, when the layered structure is bounded, or when the structure cannot be treated as a layered structure, the traditional FEM and BEM are normally required. Since a FE mesh has to be created for each layer, the calculation becomes very time-consuming, especially when the number of layers is large. A 2.5D FE model can also be established for porous material based on Biot's theory, as in Ref. [46] for sound radiation from, and absorption by, a railway track. However, since the porous material has many more degrees of freedom than a pure solid or fluid, a 2.5D FE-BE model for a structure with porous material is often too time-consuming.

1.2 Aim of the work

According to the above literature review it can be concluded that alternative approaches are still required which can be used to predict the vibro-acoustic behaviour of complex rib-stiffened panels with acoustic treatments with sufficient accuracy and efficiency. This is the main purpose of this paper. The 2.5D structural FEM, the 2.5D acoustical BEM and the transfer matrix method are combined and applied to a complex rib-stiffened panel with acoustic treatment. In Section 2, the 2.5D FE and 2.5D BE methods are introduced and coupled with the TMM. In Section 3, the accuracy and efficiency of the proposed method is quantified through comparison between results from this method and that from a full 2.5D FE-BE method for an infinitely long and acoustically treated homogeneous plate. In Section 4, the vibro-acoustic behaviour of a typical rib-stiffened panel together with an acoustic treatment layer, commonly used in train carriages, is investigated using the proposed method.

2. Formulation

An example of a long rib-stiffened panel (base panel) with a complex cross-sectional geometry is shown in Fig. 1. An acoustic treatment layer may be applied to the transmitting side of the base panel (the opposite side to the incident sound field) to increase its acoustic performance. To enable analysis at a reasonable cost while retaining accuracy, the structure needs to be simplified to some extent. The configuration is shown in Fig. 2 in which Fluid 1 is the domain from which the sound is incident and Fluid 2 is the domain to which sound is transmitted. It is assumed that the base panel is infinitely long and uniform in the longitudinal (x-) direction and has a width of $2b$ in the lateral (y-) direction. The acoustic treatment layer is normally much softer than the base panel and does not add significantly to its bending stiffness. In order to apply the TMM, it is necessary to assume that the acoustic treatment layer is also infinite in the y-direction. This approximation can be justified by the fact that the sound absorption of the layer is limited at low frequencies, so the acoustic treatment is only effective at higher frequencies at which the acoustic wavelength is shorter than the lateral dimension of the panel. Thus, TMM is applied to the acoustic treatment layer and the air beyond.

It is assumed that the acoustic treatment layer consists of N sub-layers of porous material, as shown in Fig. 3. M_{2j-1} and M_{2j}, where, $j = 1, 2, \ldots, N$, are used to represent the bottom and top surfaces of the jth sub-layer. The boundaries of the base panel interfacing with Fluid 1 and the acoustic treatment layer are, respectively, denoted by Γ_1 and Γ_2.

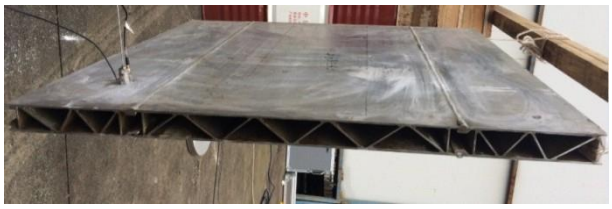

Fig. 1 A long rib-stiffened panel

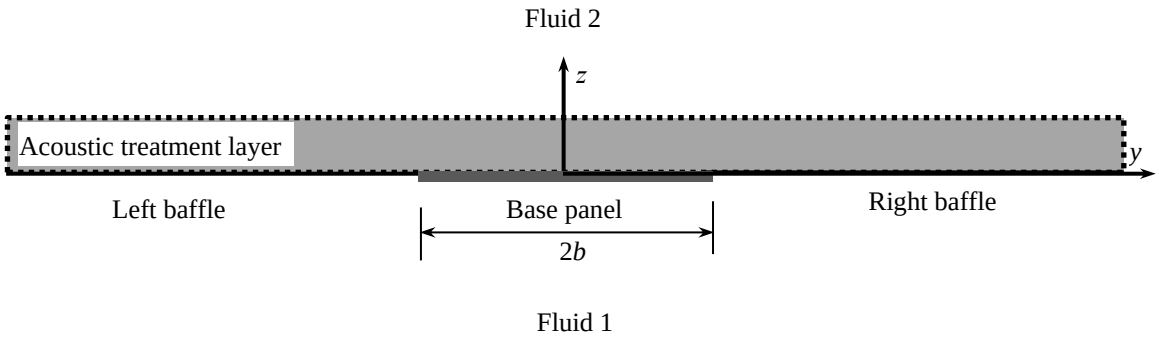

Fig. 2 A sketch of the base panel with an acoustic treatment layer. For application of TMM it is assumed that the treatment layer extends beyond the width of the panel

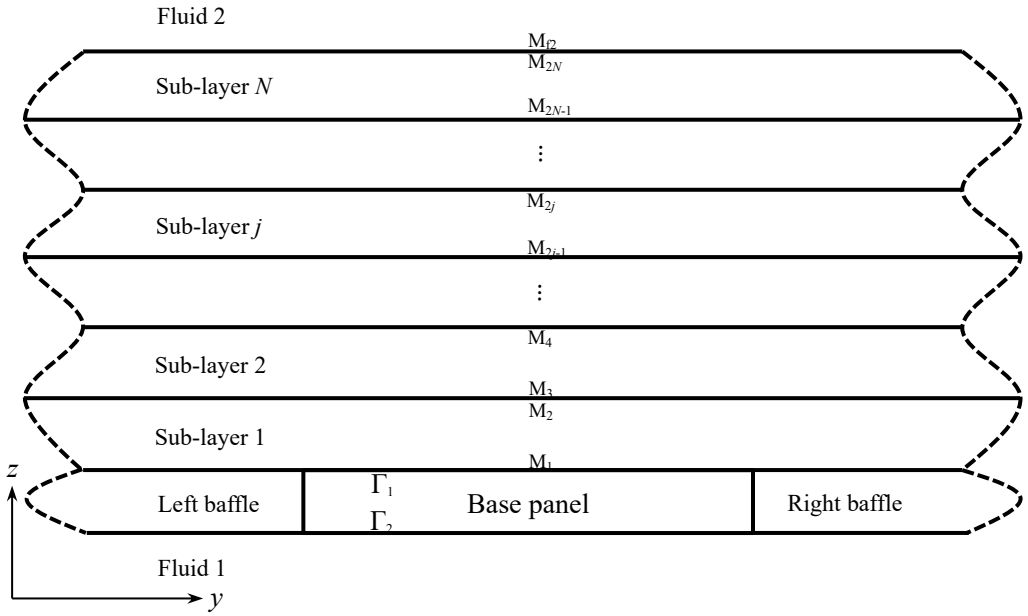

Fig. 3 A sketch of the acoustic treatment layer

An incident plane wave in Fluid 1 is assumed to impinge on the base panel in the direction of the arrow. The incident angles of the plane wave are defined in Fig. 4; φ is the angle in the yz-plane and ψ is the angle relative to the x-axis. The angle between the wave vector and the z-axis is given by $\theta = \arccos\left(\sin\psi \sin\varphi\right)$. The incident wave can be expressed as

$$p_{\mathrm{i}}(x,y,z,t) = \overline{p}_{\mathrm{i}}\, \mathrm{e}^{-\mathrm{i}k_x x} \mathrm{e}^{-\mathrm{i}k_y y} \mathrm{e}^{-\mathrm{i}k_z z} \mathrm{e}^{\mathrm{i}\omega t}, \tag{1}$$

where $\overline{p}_{\mathrm{i}}$ is the sound pressure amplitude of the incident wave and the overbar means the frequency-dependent amplitude, ω is the radian frequency, $\mathrm{i} = \sqrt{-1}$, and

$$k_x = k_1 \cos\psi, \quad k_y = k_1 \sin\psi \cos\varphi, \quad k_z = k_1 \sin\psi \sin\varphi, \tag{2}$$

are wavenumbers in the x-, y- and z-direction, with k_1 being the acoustic wavenumber in Fluid 1.

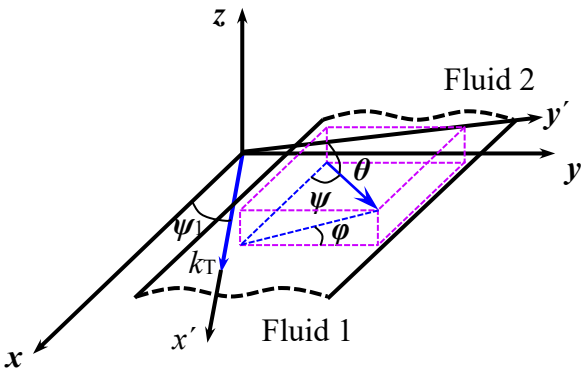

Fig. 4 Definition of the incident angle of the incident plane wave and that of the wavenumber vector (k_T) of a vibration wave propagating in the acoustic treatment layer

In the remainder of this section, the 2.5D FE method, the Rayleigh integral-based 2.5D BE method, the transfer matrix method and the coupling between them are introduced. The 2.5D FE-BE method for the base panel plus Fluid 1 is described in Section 2.1, the TMM for the acoustic treatment layer plus Fluid 2 is described in Section 2.2, the coupling of the base panel with the acoustic treatment layer is described in Section 2.3, and the calculation of sound radiation and sound transmission loss of the acoustically treated panel is introduced in Section 2.4.

2.1 The 2.5D FE-BE method for the base panel plus Fluid 1

Since the base panel has a complex cross-sectional geometry and is uniform and infinitely long in the x-direction, its vibration can be modelled using the 2.5D FEM. For temporally (with radian frequency ω) and spatially (in the x-direction with wavenumber k_x) harmonic excitation, the 2.5D FE equation governing vibration of the base panel is given by [37]

$$\left[\mathbf{K}\left(k_x\right)-\omega^2\mathbf{M}\right]\bar{\mathbf{q}}=\bar{\mathbf{F}}, \tag{3}$$

where $\bar{\mathbf{q}}$ is the vector of nodal displacement amplitudes, $\bar{\mathbf{F}}$ is the associated vector of nodal force amplitudes, $\mathbf{M}$ is a symmetric and positive mass matrix, and

$$\mathbf{K}\left(k_x\right)=\mathbf{K}_0+\left(-\mathrm{i}k_x\right)\mathbf{K}_1+\left(-\mathrm{i}k_x\right)^2\mathbf{K}_2+\left(-\mathrm{i}k_x\right)^4\mathbf{K}_4, \tag{4}$$

where $\mathbf{K}_0$ is a symmetric and non-negative matrix, $\mathbf{K}_1$ is an anti-symmetric matrix, $\mathbf{K}_2$ is a symmetric and positive matrix. If all the degrees of freedom consist of translational displacements, then $\mathbf{K}_4 = \mathbf{0}$, otherwise it is a symmetric matrix. The nodal force vector corresponding to the fluid loading from Fluid 1 and other forces (due to tractions at the interface with the acoustic treatment) can be calculated as

$$\bar{\mathbf{F}}=\int_{\Gamma_1}\mathbf{N}_\mathrm{p}^\mathrm{T}\left(0,0,\bar{p}_\mathrm{i}+\bar{p}_\mathrm{r1}\right)^\mathrm{T}\mathrm{d}\Gamma+\left(\int_{\Gamma_1}\mathbf{N}_\mathrm{p}^\mathrm{T}\mathbf{N}'_{\mathrm{r}2}\mathrm{d}\Gamma\right)\bar{\mathbf{p}}_{\mathrm{r}2}+\int_{\Gamma_1+\Gamma_2}\mathbf{N}_\mathrm{p}^\mathrm{T}\bar{\mathbf{F}}_\mathrm{e}\mathrm{d}\Gamma, \tag{5}$$

where $\bar{p}_{\mathrm{r}1}$ is the sound pressure amplitude of the rigidly reflected wave in Fluid 1 (i.e. as if the base panel were rigid), given by

$$p_{\mathrm{r}1}(x,y,z,t)=\bar{p}_{\mathrm{r}1}\mathrm{e}^{-\mathrm{i}k_x x}\mathrm{e}^{-\mathrm{i}k_y y}\mathrm{e}^{\mathrm{i}k_z z}\mathrm{e}^{\mathrm{i}\omega t}; \tag{6}$$

$\bar{\mathbf{p}}_{\mathrm{r}2}$ is the vector of nodal pressure amplitudes of the sound wave on Γ_1, radiated by vibration of the baffled base panel; $\bar{\mathbf{F}}_\mathrm{e}$ represents other forces (tractions) externally applied on the panel surfaces;

$\mathbf{N}_\mathrm{p}$ and $\mathbf{N}'_{\mathrm{r}2}$ are shape function matrices. By letting

$$\bar{\mathbf{F}}_\mathrm{f} = \int_{\Gamma_1} \mathbf{N}_\mathrm{p}^\mathrm{T} \left(0, 0, \bar{p}_\mathrm{i} + \bar{p}_{\mathrm{r}1}\right)^\mathrm{T} \mathrm{d}\Gamma\,, \qquad \mathbf{C}_{\mathrm{r}2} = \int_{\Gamma_1} \mathbf{N}_\mathrm{p}^\mathrm{T} \mathbf{N}'_{\mathrm{r}2} \mathrm{d}\Gamma\,, \qquad \bar{\mathbf{F}}_\mathrm{s} = \int_{\Gamma_1+\Gamma_2} \mathbf{N}_\mathrm{p}^\mathrm{T} \bar{\mathbf{F}}_\mathrm{e} \mathrm{d}\Gamma\,, \tag{7}$$

Eq. (3) becomes

$$\left[\mathbf{K}\left(k_x\right) - \omega^2 \mathbf{M}\right] \bar{\mathbf{q}} - \mathbf{C}_{\mathrm{r}2} \bar{\mathbf{p}}_{\mathrm{r}2} = \bar{\mathbf{F}}_\mathrm{f} + \bar{\mathbf{F}}_\mathrm{s}\,, \tag{8}$$

Since the normal velocities of the base panel on the boundary Γ_1 must be equal to those of Fluid 1, one has

$$\mathrm{i}\omega \mathbf{E}_{\mathrm{r}2} \bar{\mathbf{q}} = \bar{\mathbf{v}}_{\mathrm{r}2\mathrm{n}}\,, \tag{9}$$

where $\mathbf{E}_{\mathrm{r}2}$ is a matrix transforming the nodal velocity vector of the base panel to the normal velocity vector on Γ_1, and $\bar{\mathbf{v}}_{\mathrm{r}2\mathrm{n}}$ is the vector of nodal normal velocity amplitudes in the fluid on Γ_1, corresponding to $\bar{\mathbf{p}}_{\mathrm{r}2}$.

The relationship between sound pressure and particle velocity on the structure/fluid interface is now utilised. Here, use is made of the 2.5D Rayleigh integral [38], i.e.

$$\bar{p}\left(\mathbf{r}\right) = \frac{\mathrm{i}\rho_0 \omega}{\pi} \int_{\Gamma_1} \bar{v}_\mathrm{n}\left(\mathbf{r}'\right) \mathrm{K}_0\left(\kappa \left|\mathbf{r} - \mathbf{r}'\right|\right) \mathrm{d}\Gamma_1\,, \tag{10}$$

where $\bar{v}_\mathrm{n}\left(\mathbf{r}'\right)$ is the normal particle velocity amplitude in Fluid 1 at position $\mathbf{r}'$ on Γ_1, with the normal pointing into the fluid domain; K_0 is the 0th order modified Bessel function of the second kind; $\kappa = \sqrt{k_x^2 - k_1^2}$ and as before k_x is the wavenumber in the x-direction.

Applying the same shape function as used for the fluid pressure to the fluid normal velocity on boundary Γ_1, and writing Eq. (10) for each node, gives an equation that can be written in the form

$$\mathbf{H}_{\mathrm{r}2} \bar{\mathbf{p}}_{\mathrm{r}2} - \mathbf{G}_{\mathrm{r}2} \bar{\mathbf{v}}_{\mathrm{r}2\mathrm{n}} = \mathbf{0}\,. \tag{11}$$

Combining Eqs. (8), (9) and (11) gives

$$\begin{bmatrix} \mathbf{0} & -\lambda \mathbf{C}_{\mathrm{r}2} & \mathbf{K}\left(k_x\right) - \omega^2 \mathbf{M} \\ \lambda \mathbf{I} & \mathbf{0} & -\mathrm{i}\omega \mathbf{E}_{\mathrm{r}2} \\ -\lambda \mathbf{G}_{\mathrm{r}2} & \lambda \mathbf{H}_{\mathrm{r}2} & \mathbf{0} \end{bmatrix} \begin{bmatrix} \bar{\mathbf{v}}_{\mathrm{r}2\mathrm{n}} \\ \bar{\mathbf{p}}_{\mathrm{r}2\mathrm{n}} \\ \lambda \bar{\mathbf{q}} \end{bmatrix} = \begin{bmatrix} \lambda\left(\bar{\mathbf{F}}_\mathrm{f} + \bar{\mathbf{F}}_\mathrm{s}\right) \\ \mathbf{0} \\ \mathbf{0} \end{bmatrix}. \tag{12}$$

A constant λ is introduced in Eq. (12) to scale the coefficient matrix and avoid it becoming highly ill conditioned due to a difference of almost ten orders of magnitude between the first two columns (for the fluid) and the last one (for the structure).

2.2 The TMM for the acoustic treatment layer plus Fluid 2

The TMM [45] is applied to the multiple layer acoustic treatment and the Fluid 2 acoustic domain. To apply the TMM it is necessary to take a two-dimensional Fourier transform over x and y, which implies that the acoustic treatment also extends to cover the baffle. It is therefore assumed that a vibration and/or acoustic wave, with x-wavenumber component denoted by k'_x and y-wavenumber component denoted by k'_y, is propagating in the acoustic treatment layer, as shown in Fig. 4. Thus the wavenumber in the xy-plane is $k_{\mathrm{T}} = \sqrt{k_x'^2 + k_y'^2}$ and the included angle of the wave vector with the x-axis is given by $\psi_1 = \arctan\left(k'_y / k'_x\right)$. It is further assumed that any horizontal shear waves can be neglected since they do not contribute to the sound radiation. When the acoustic treatment layer is coupled with the base panel, $k'_x = k_x$. The coordinate system $oxyz$ is now rotated around the z-axis by angle ψ_1 to form a new coordinate system $ox'y'z$ that depends on k'_y. In the new coordinate system, the x'-axis coincides with the direction of the wave vector in the xy-plane, and velocities and stresses in the y'-direction are all equal to zero (because the horizontal shear waves are neglected). Thus, the response of the acoustic treatment layer associated with the above wave can be handled in the $x'z$-plane using TMM as a two-dimensional problem.

According to TMM [45], a series of layers are considered which may be elastic, poro-rigid, poro-elastic or fluid. The equation governing the vibration of the acoustic treatment layer and the air beyond can be expressed in a general form as

$$\left[\begin{array}{ccccccc:c}
\mathbf{I}_{1,2}\mathbf{T}_1 & \mathbf{J}_{1,2} & \mathbf{0} & \mathrm{L} & \mathbf{0} & \mathbf{0} & \mathbf{0} & \\
\mathbf{0} & \mathbf{I}_{2,3}\mathbf{T}_2 & \mathbf{J}_{2,3} & \mathrm{L} & \mathbf{0} & \mathbf{0} & \mathbf{0} & \\
\mathrm{M} & \mathrm{M} & \mathrm{M} & & \mathrm{M} & \mathrm{M} & \mathrm{M} & \\
\mathbf{0} & \mathbf{0} & \mathbf{0} & \mathrm{L} & \mathbf{I}_{(N\text{-}1),N}\mathbf{T}_{N-1} & \mathbf{J}_{(N\text{-}1),N} & \mathbf{0} & \\
\mathbf{0} & \mathbf{0} & \mathbf{0} & \mathrm{L} & \mathbf{0} & \mathbf{I}_{N,\mathrm{f2}}\mathbf{T}_N & \mathbf{J}_{N,\mathrm{f2}} & \\
\hdashline
0 & 0 & 0 & \mathrm{L} & 0 & 0 & -1 & Z_{\mathrm{f2}}
\end{array}\right] \mathbf{V} = \mathbf{0}, \tag{13}$$

where $\mathbf{I}_{j,(j+1)}$ and $\mathbf{J}_{j,(j+1)}$ (j = 1, 2, …, N-1) are matrices representing stress balance and velocity continuity at the interface between the jth layer and the (j+1)th layer. Elements in these matrices are either 0, 1, -1 or equal to the porosity of the associated porous material; similarly, matrices $\mathbf{I}_{N,\mathrm{f2}}$ and $\mathbf{J}_{N,\mathrm{f2}}$ are the corresponding stress and velocity relation at the interface between the Nth layer and Fluid 2. Matrix $\mathbf{T}_j$ (j = 1, 2, …, N) is the transfer matrix of the jth layer; Z_{f2} is the normal characteristic impedance of Fluid 2 (as a half-space) at the interface and it can be calculated as

$$Z_{f2} = \frac{\omega \rho_2}{k_z'}, \tag{14}$$

where $k_z' = \sqrt{k_2^2 - k_x'^2 - k_y'^2}$ is the acoustic wavenumber of Fluid 2 in the z-direction; k_2 is the acoustic wavenumber of Fluid 2; ρ_2 is the density of Fluid 2. $\mathbf{v}$ in Eq. (13) is the combined stress and velocity vector, given by

$$\mathbf{v} = \left[\mathbf{v}_1(\mathrm{M}_1)^{\mathrm{T}} \quad \mathbf{v}_2(\mathrm{M}_3)^{\mathrm{T}} \quad \mathbf{v}_3(\mathrm{M}_5)^{\mathrm{T}} \quad \mathrm{L} \quad \mathbf{v}_{N-1}\left(\mathrm{M}_{2(N-1)-1}\right)^{\mathrm{T}} \quad \mathbf{v}_N(\mathrm{M}_{2N-1})^{\mathrm{T}} \;\vdots\; \mathbf{v}_{f2}(\mathrm{M}_{f2})^{\mathrm{T}} \right]^{\mathrm{T}}. \tag{15}$$

where $\mathbf{v}_j\left(\mathrm{M}_{2j-1}\right)$ (j = 1, 2, …, N) is the state vector including stress and velocity components of the jth layer at M_{2j-1}, in which the number of elements depends on how the absorptive material in the layer is modelled. If the jth layer is simulated with a poro-elastic model, the state vector is expressed as

$$\mathbf{v}_j(\mathrm{M}) = \left[v_x^s(\mathrm{M}) \quad v_z^s(\mathrm{M}) \quad v_z^f(\mathrm{M}) \quad \sigma_{zz}^s(\mathrm{M}) \quad \sigma_{xz}^s(\mathrm{M}) \quad \sigma_{zz}^f(\mathrm{M}) \right]^{\mathrm{T}}, \tag{16}$$

where M represents a plane parallel to the $x'y'$-plane in the jth layer, v and σ are the velocity and stress, respectively, and superscripts ‘s’ and ‘f’ represent, respectively, the corresponding velocity or stress of the solid phase (frame) and fluid phase of the porous material. On the other hand, if the jth layer is simulated with a poro-rigid model, the porous layer can be treated as a layer of an equivalent fluid, and the state vector is expressed as

$$\mathbf{v}_j(\mathrm{M}) = \left[p_{eq}^f(\mathrm{M}) \quad v_{z,eq}^f(\mathrm{M}) \right]^{\mathrm{T}}, \tag{17}$$

where $p_{eq}^f(\mathrm{M})$ is the fluid pressure of the equivalent fluid at M. For the equivalent fluid, the mass of the porous material and vibration of the frame are not taken into account. Similar to the equivalent fluid layer, the state vector of Fluid 2, as a half-space, is expressed as

$$\mathbf{v}_{f2}(\mathrm{M}) = \left[p^{f2}(\mathrm{M}) \quad v_z^{f2}(\mathrm{M}) \right]^{\mathrm{T}}, \tag{18}$$

It is worth noting that the coefficient matrix of Eq. (13) is not square since the traction and displacement restraints at the interface of the first sub-layer layer with the base panel and baffles have not been considered yet. It is assumed that the state vector $\mathbf{v}$ is of dimension n×1, which varies depending on which models are used for the sub-layers of the acoustic treatment. Therefore, the dimensions of the coefficient matrix in Eq. (13) depend on which model is adopted for the first sub-layer. If the first sub-layer is simulated by a poro-elastic model, the coefficient matrix is of

dimension (n-3)×n. If the first sub-layer is simulated by a poro-rigid model, it is of dimension (n-1)×n.

When the first sub-layer is poro-elastic, since the acoustic treatment layer interacts with the base panel, the normal velocities of the solid and fluid of the acoustic treatment at M_1 must be identical to each other (and therefore is denoted by $v_z^s(M_1) - v_z^f(M_1) = 0$); the total normal stress, denoted by $\sigma_{zz}^s(M_1) + \sigma_{zz}^f(M_1)$, and the total tangential stress, denoted by $\sigma_{xz}^s(M_1)$ of the acoustic treatment at M_1 must be equal to the traction applied by the base panel and baffles in the z- and x'-direction, respectively. These conditions may be written in the form

$$\mathbf{Y}\mathbf{v}_1(M_1) = \mathbf{t}, \tag{19}$$

where

$$\mathbf{Y} = \begin{bmatrix} 0 & 1 & -1 & 0 & 0 & 0 \\ 0 & 0 & 0 & 0 & 1 & 0 \\ 0 & 0 & 0 & 1 & 0 & 1 \end{bmatrix}, \tag{20}$$

$$\mathbf{t} = \begin{bmatrix} 0 \\ -\mathbf{E}_1\mathbf{t}_0 \end{bmatrix}, \tag{21}$$

in which $\mathbf{t}_0(k_x, k_y') = (p_x, 0, p_z)^{\mathrm{T}}$ is the Fourier-transformed or wavenumber domain traction applied by the base panel and baffles to the acoustic treatment layer, and

$$\mathbf{E}_1 = \begin{bmatrix} 1 & 0 & 0 \\ 0 & 0 & 1 \end{bmatrix}. \tag{22}$$

When the first sub-layer is poro-rigid, matrices $\mathbf{Y}$ and $\mathbf{t}$ reduce to

$$\mathbf{Y} = \begin{bmatrix} 1 & 0 \end{bmatrix}, \tag{23}$$

$$\mathbf{t} = \mathbf{E}_2\mathbf{t}_0, \tag{24}$$

where

$$\mathbf{E}_2 = \begin{bmatrix} 0 & 0 & 1 \end{bmatrix}. \tag{25}$$

Combining Eq. (13) with Eq. (19) gives

$$\left[\begin{array}{cccccc:c} \mathbf{Y} & \mathbf{0} & \mathbf{0} & \mathrm{L} & \mathbf{0} & \mathbf{0} & \mathbf{0} \\ \mathbf{I}_{1,2}\mathbf{T}_1 & \mathbf{J}_{1,2} & \mathbf{0} & \mathrm{L} & \mathbf{0} & \mathbf{0} & \mathbf{0} \\ \mathbf{0} & \mathbf{I}_{2,3}\mathbf{T}_2 & \mathbf{J}_{2,3} & \mathrm{L} & \mathbf{0} & \mathbf{0} & \mathbf{0} \\ \mathrm{M} & \mathrm{M} & \mathrm{M} & & \mathrm{M} & \mathrm{M} & \mathrm{M} \\ \mathbf{0} & \mathbf{0} & \mathbf{0} & \mathrm{L} & \mathbf{I}_{(N\text{-}1),N}\mathbf{T}_{N-1} & \mathbf{J}_{(N\text{-}1),N} & \mathbf{0} \\ \mathbf{0} & \mathbf{0} & \mathbf{0} & \mathrm{L} & \mathbf{0} & \mathbf{I}_{N,\mathrm{f}2}\mathbf{T}_N & \mathbf{J}_{N,\mathrm{f}2} \\ \hdashline 0 & 0 & 0 & \mathrm{L} & 0 & 0 & -1 \quad Z_{\mathrm{f}2} \end{array}\right] \left[\begin{array}{c} \mathbf{V}_1 \\ \mathbf{V}_2 \\ \mathbf{V}_3 \\ \mathrm{M} \\ \mathbf{V}_N \\ \mathbf{V}_{N+1} \\ \hdashline v_{\mathrm{f}2} \end{array}\right] = \left[\begin{array}{c} \mathbf{f}_1 \\ \mathbf{0} \\ \mathbf{0} \\ \mathrm{M} \\ \mathbf{0} \\ \mathbf{0} \\ \hdashline 0 \end{array}\right]. \tag{26}$$

With Eq. (26), the Fourier-transformed velocity of the acoustic treatment layer at the interface with the base panel and baffles can be expressed as a function of $\mathbf{f}_1$, i.e.

$$\mathbf{V}_1 = \mathbf{R}^{\mathrm{d}}\mathbf{f}_1, \tag{27}$$

where $\mathbf{V}_1 = (v_x, 0, v_z)^{\mathrm{T}}$; $\mathbf{R}^{\mathrm{d}}$ is called the Fourier-transformed dynamic mobility matrix of the acoustic treatment layer at the interface in the coordinate system *ox'y'z*, and it is formed of elements of the inverse of the coefficient matrix in Eq. (26).

$\mathbf{R}^{\mathrm{d}}$ in Eq. (27) is derived in terms of the coordinate system *ox'y'z*. It can be transformed into the *oxyz* coordinate system. The relationships of velocities and tractions between the two coordinate systems are expressed as

$$\mathbf{V}_1 = \mathbf{T}\mathbf{V}_0, \tag{28}$$

$$\mathbf{f}_1 = \mathbf{T}\mathbf{f}_0, \tag{29}$$

where $\mathbf{V}_0$ and $\mathbf{f}_0$ are the corresponding velocity and traction in the coordinate system *oxyz*, and

$$\mathbf{T} = \begin{bmatrix} \cos\psi_1 & -\sin\psi_1 & 0 \\ \sin\psi_1 & \cos\psi_1 & 0 \\ 0 & 0 & 1 \end{bmatrix}. \tag{30}$$

Substituting Eqs. (28) and (29) into Eq. (27) gives the Fourier-transformed dynamic mobility matrix of the acoustic treatment layer at the panel/acoustic treatment interface in the coordinate system *oxyz* as

$$\mathbf{R}^{\mathrm{d}}_0 = \mathbf{T}^{\mathrm{T}}\mathbf{R}^{\mathrm{d}}\mathbf{T}. \tag{31}$$

Thus, the Fourier-transformed dynamic flexibility matrix in the coordinate system *oxyz* can be calculated as

$$\mathbf{Q}^{\mathrm{d}}_0 = \mathbf{R}^{\mathrm{d}}_0 / \mathrm{i}\omega, \tag{32}$$

which is useful for finding the displacement at the interface of the acoustic treatment layer with the base panel and baffles in the coordinate system *oxyz* when the traction is known. This displacement

will be used in Section 2.3 as one of the coupling conditions, i.e. the displacement continuity at the interface.

2.3 Coupling of the base panel with the acoustic treatment layer

To couple the 2.5D FE model to the TMM, the response at the interface nodes has to be expressed as a Fourier transform over wavenumber k_y. It is assumed that, in the 2.5D FE model of the base panel presented in Section 2.1, there are N_0 nodes on the interface (denoted by B_0) between the base panel and the acoustic treatment layer. The y-coordinates of these nodes are denoted by y_j^0, where, $j = 1, 2, \ldots N_0$. The displacement on the interface can be expressed as

$$\mathbf{w}_0(x,y,t) = \bar{\mathbf{w}}_0(y)\mathrm{e}^{\mathrm{i}(\omega t - k_x x)} = \mathbf{\Phi}_0(y)\bar{\mathbf{q}}_0\mathrm{e}^{\mathrm{i}(\omega t - k_x x)},\ (-b \le y \le b) \tag{33}$$

where

$$\bar{\mathbf{q}}_0 = \begin{Bmatrix} \bar{\mathbf{w}}_1^0 \\ \cdots \\ \bar{\mathbf{w}}_{N_0}^0 \end{Bmatrix}, \tag{34}$$

is the vector of nodal displacements on B_0, and $\mathbf{\Phi}_0(y)$ is a shape function matrix. Similarly, the tractions applied by the base panel to the acoustic treatment can be expressed as

$$\boldsymbol{\tau}_0(x,y,t) = \bar{\boldsymbol{\tau}}_0(y)\mathrm{e}^{\mathrm{i}(\omega t - k_x x)} = \mathbf{\Phi}_0(y)\bar{\mathbf{p}}_0\mathrm{e}^{\mathrm{i}(\omega t - k_x x)},\ (-b \le y \le b) \tag{35}$$

where

$$\bar{\mathbf{p}}_0 = \begin{Bmatrix} \bar{\boldsymbol{\tau}}_1^0 \\ \cdots \\ \bar{\boldsymbol{\tau}}_{N_0}^0 \end{Bmatrix}, \tag{36}$$

is the vector of nodal tractions on B_0.

As shown in Fig. 2, the acoustic treatment layer is assumed to extend beyond the panel and is connected to the baffle in this region. The left (right) interface between the acoustic treatment layer and the baffle is denoted by B_L (B_R). There are N_L (N_R) nodes on this interface, covering a truncated width of b^*. The y-coordinate of the kth node is denoted by y_k^- (y_k^+), where $-b-b^* \le y_k^- < -b$ ($b < y_k^+ \le b+b^*$). This implies that tractions on the interface vanish when $|y| > b+b^*$. It is assumed

that B_L (B_R) has no displacement, while the traction applied to the acoustic treatment layer is denoted by $\bar{\boldsymbol{\tau}}_{\mathrm{L}}(y)$ ($\bar{\boldsymbol{\tau}}_{\mathrm{R}}(y)$). Similar to Eq. (35), this can be written as

$$\bar{\boldsymbol{\tau}}_{\mathrm{L}}(y)=\boldsymbol{\Phi}_{\mathrm{L}}(y)\bar{\mathbf{p}}_{\mathrm{L}},\quad \bar{\boldsymbol{\tau}}_{\mathrm{R}}(y)=\boldsymbol{\Phi}_{\mathrm{R}}(y)\bar{\mathbf{p}}_{\mathrm{R}}, \tag{37}$$

where

$$\bar{\mathbf{p}}_{\mathrm{L}}=\begin{Bmatrix}\bar{\boldsymbol{\tau}}_1^{\mathrm{L}}\\ \vdots\\ \bar{\boldsymbol{\tau}}_{N_{\mathrm{L}}}^{\mathrm{L}}\end{Bmatrix},\qquad \bar{\mathbf{p}}_{R}=\begin{Bmatrix}\bar{\boldsymbol{\tau}}_1^{\mathrm{R}}\\ \vdots\\ \bar{\boldsymbol{\tau}}_{N_{\mathrm{R}}}^{\mathrm{R}}\end{Bmatrix}, \tag{38}$$

are the nodal traction vectors, and $\boldsymbol{\Phi}_{\mathrm{L}}(y)$ and $\boldsymbol{\Phi}_{\mathrm{R}}(y)$ are two shape function matrices.

The Fourier transform of the tractions applied by the base panel and baffles to the acoustic treatment layer is given by

$$\tilde{\boldsymbol{\tau}}(k_x,k_y')=\int_{-\infty}^{-b}\bar{\boldsymbol{\tau}}_{\mathrm{L}}(y)\mathrm{e}^{-\mathrm{i}k_y'y}\mathrm{d}y+\int_{b}^{\infty}\bar{\boldsymbol{\tau}}_{\mathrm{R}}(y)\mathrm{e}^{-\mathrm{i}k_y'y}\mathrm{d}y+\int_{-b}^{\mathrm{b}}\bar{\boldsymbol{\tau}}_{0}(y)\mathrm{e}^{-\mathrm{i}k_y'y}\mathrm{d}y, \tag{39}$$

or, with truncation of the baffle/acoustic treatment layer interface,

$$\begin{aligned}\tilde{\boldsymbol{\tau}}(k_x,k_y')&=\left(\int_{-b^*}^{-b}\boldsymbol{\Phi}_{\mathrm{L}}(y)\mathrm{e}^{-\mathrm{i}k_y'y}\mathrm{d}y\right)\bar{\mathbf{p}}_{\mathrm{L}}+\left(\int_{b}^{b^*}\boldsymbol{\Phi}_{\mathrm{R}}(y)\mathrm{e}^{-\mathrm{i}k_y'y}\mathrm{d}y\right)\bar{\mathbf{p}}_{\mathrm{R}}+\left(\int_{-b}^{b}\boldsymbol{\Phi}_{0}(y)\mathrm{e}^{-\mathrm{i}k_y'y}\mathrm{d}y\right)\bar{\mathbf{p}}_{0}\\ &=\tilde{\boldsymbol{\Phi}}_{\mathrm{L}}(k_y')\bar{\mathbf{p}}_{\mathrm{L}}+\tilde{\boldsymbol{\Phi}}_{\mathrm{R}}(k_y')\bar{\mathbf{p}}_{\mathrm{R}}+\tilde{\boldsymbol{\Phi}}_{0}(k_y')\bar{\mathbf{p}}_{0}\end{aligned}. \tag{40}$$

Therefore, with the Fourier-transformed dynamic flexibility matrix $\tilde{\mathbf{Q}}$ established in Section 2.2, the Fourier-transformed displacement of the acoustic treatment layer at the interface with the base panel and baffles is

$$\tilde{\mathbf{w}}(k_x,k_y')=\tilde{\mathbf{Q}}(k_x,k_y')\tilde{\boldsymbol{\tau}}(k_x,k_y'). \tag{41}$$

Thus, the displacement of the acoustic treatment layer at the interface can be calculated as

$$\begin{aligned}\mathbf{w}(k_x,y)&=\frac{1}{2\pi}\int_{-\infty}^{\infty}\tilde{\mathbf{w}}(k_x,k_y')\mathrm{e}^{\mathrm{i}k_y'y}\mathrm{d}k_y'\\ &=\frac{1}{2\pi}\int_{-\infty}^{\infty}\tilde{\mathbf{Q}}(k_x,k_y')\tilde{\boldsymbol{\tau}}(k_x,k_y')\mathrm{e}^{\mathrm{i}k_y'y}\mathrm{d}k_y'\\ &=\mathbf{A}_{\mathrm{L}}(y)\bar{\mathbf{p}}_{\mathrm{L}}+\mathbf{A}_{\mathrm{R}}(y)\bar{\mathbf{p}}_{\mathrm{R}}+\mathbf{A}_{0}(y)\bar{\mathbf{p}}_{0}\end{aligned}, \tag{42}$$

where

$$\mathbf{A}_{\mathrm{L}}\left(y\right)=\frac{1}{2\pi}\int_{-\infty}^{\infty}\tilde{\mathbf{Q}}(k_x,k_y')\tilde{\mathbf{\Phi}}_{\mathrm{L}}(k_y')\mathrm{e}^{\mathrm{i}k_y'y}\mathrm{d}k_y', \tag{43}$$

$$\mathbf{A}_{\mathrm{R}}\left(y\right)=\frac{1}{2\pi}\int_{-\infty}^{\infty}\tilde{\mathbf{Q}}(k_x,k_y')\tilde{\mathbf{\Phi}}_{\mathrm{R}}(k')\mathrm{e}^{\mathrm{i}k_y'y}\mathrm{d}k_y', \tag{44}$$

$$\mathbf{A}_{0}\left(y\right)=\frac{1}{2\pi}\int_{-\infty}^{\infty}\tilde{\mathbf{Q}}(k_x,k_y')\tilde{\mathbf{\Phi}}_{0}(k_y')\mathrm{e}^{\mathrm{i}k_y'y}\mathrm{d}k_y'. \tag{45}$$

Eq. (42) will be used to ensure displacement continuity at the interface of the acoustic treatment layer with the base panel and baffles. Writing Eq. (42) for each node on interfaces B_L, B_R and B_0 gives

$$\mathbf{A}_{\mathrm{L}}\left(y_k^-\right)\bar{\mathbf{p}}_{\mathrm{L}}+\mathbf{A}_{\mathrm{R}}\left(y_k^-\right)\bar{\mathbf{p}}_{\mathrm{R}}+\mathbf{A}_{0}\left(y_k^-\right)\bar{\mathbf{p}}_{0}=\mathbf{0}, \qquad (k=1,\ldots N_{\mathrm{L}}) \tag{46}$$

$$\mathbf{A}_{\mathrm{L}}\left(y_k^+\right)\bar{\mathbf{p}}_{\mathrm{L}}+\mathbf{A}_{\mathrm{R}}\left(y_k^+\right)\bar{\mathbf{p}}_{\mathrm{R}}+\mathbf{A}_{0}\left(y_k^+\right)\bar{\mathbf{p}}_{0}=\mathbf{0}, \qquad (k=1,\ldots N_{\mathrm{R}}) \tag{47}$$

$$\mathbf{A}_{\mathrm{L}}\left(y_j^0\right)\bar{\mathbf{p}}_{\mathrm{L}}+\mathbf{A}_{\mathrm{R}}\left(y_j^0\right)\bar{\mathbf{p}}_{\mathrm{R}}+\mathbf{A}_{0}\left(y_j^0\right)\bar{\mathbf{p}}_{0}=\bar{\mathbf{w}}_j^0, \qquad (j=1,\ldots N_0) \tag{48}$$

Eqs. (46), (47) and (48) can be written in the compact form

$$\begin{bmatrix}\mathbf{A}_{\mathrm{L}}^- & \mathbf{A}_{\mathrm{R}}^- & \mathbf{A}_{0}^-\\ \mathbf{A}_{\mathrm{L}}^+ & \mathbf{A}_{\mathrm{R}}^+ & \mathbf{A}_{0}^+\\ \mathbf{A}_{\mathrm{L}}^0 & \mathbf{A}_{\mathrm{R}}^0 & \mathbf{A}_{0}^0\end{bmatrix}\begin{bmatrix}\bar{\mathbf{p}}_{\mathrm{L}}\\ \bar{\mathbf{p}}_{\mathrm{R}}\\ \bar{\mathbf{p}}_{0}\end{bmatrix}=\begin{bmatrix}\mathbf{0}\\ \mathbf{0}\\ \bar{\mathbf{q}}_{0}\end{bmatrix}, \tag{49}$$

where

$$\mathbf{A}_L^-=\left[\mathbf{A}_L\left(y_1^-\right)^{\mathrm{T}}\ \ \mathrm{L}\ \ \mathbf{A}_L\left(y_{N_L}^-\right)^{\mathrm{T}}\right]^{\mathrm{T}},\ \mathbf{A}_R^-=\left[\mathbf{A}_R\left(y_1^-\right)^{\mathrm{T}}\ \ \mathrm{L}\ \ \mathbf{A}_R\left(y_{N_L}^-\right)^{\mathrm{T}}\right]^{\mathrm{T}},\ \mathbf{A}_0^-=\left[\mathbf{A}_0\left(y_1^-\right)^{\mathrm{T}}\ \ \mathrm{L}\ \ \mathbf{A}_0\left(y_{N_L}^-\right)^{\mathrm{T}}\right]^{\mathrm{T}},$$

$$\mathbf{A}_L^+=\left[\mathbf{A}_L\left(y_1^+\right)^{\mathrm{T}}\ \ \mathrm{L}\ \ \mathbf{A}_L\left(y_{N_R}^+\right)^{\mathrm{T}}\right]^{\mathrm{T}},\ \mathbf{A}_R^+=\left[\mathbf{A}_R\left(y_1^+\right)^{\mathrm{T}}\ \ \mathrm{L}\ \ \mathbf{A}_R\left(y_{N_R}^+\right)^{\mathrm{T}}\right]^{\mathrm{T}},\ \mathbf{A}_0^+=\left[\mathbf{A}_0\left(y_1^+\right)^{\mathrm{T}}\ \ \mathrm{L}\ \ \mathbf{A}_0\left(y_{N_R}^+\right)^{\mathrm{T}}\right]^{\mathrm{T}},$$

$$\mathbf{A}_L^0=\left[\mathbf{A}_L\left(y_1^0\right)^{\mathrm{T}}\ \ \mathrm{L}\ \ \mathbf{A}_L\left(y_{N_0}^0\right)^{\mathrm{T}}\right]^{\mathrm{T}},\ \mathbf{A}_R^0=\left[\mathbf{A}_R\left(y_1^0\right)^{\mathrm{T}}\ \ \mathrm{L}\ \ \mathbf{A}_R\left(y_{N_0}^0\right)^{\mathrm{T}}\right]^{\mathrm{T}},\ \mathbf{A}_0^0=\left[\mathbf{A}_0\left(y_1^0\right)^{\mathrm{T}}\ \ \mathrm{L}\ \ \mathbf{A}_0\left(y_{N_{LR}}^0\right)^{\mathrm{T}}\right]^{\mathrm{T}}. \tag{50}$$

The displacement continuity at the base panel/acoustic treatment layer gives

$$\bar{\mathbf{q}}_0=\mathbf{E}_{\mathrm{t}}\bar{\mathbf{q}}, \tag{51}$$

where $\mathbf{E}_{\mathrm{t}}$ is a matrix reducing the nodal displacement vector of the base panel to one which is associated only with nodes on the base panel/acoustic treatment layer interface.

The nodal forces equivalent to the traction applied by the acoustic treatment layer to the base panel are given by

$$\bar{\mathbf{F}}_{\mathrm{T}} = -\int_{\Gamma_2} \mathbf{N}_{\mathrm{p}}^{\mathrm{T}} \bar{\boldsymbol{\tau}}_0 \mathrm{d}\Gamma_2 = -\left(\int_{\Gamma_2} \mathbf{N}_{\mathrm{p}}^{\mathrm{T}} \boldsymbol{\Phi}_0 \mathrm{d}\Gamma_2\right) \bar{\mathbf{p}}_0 . \tag{52}$$

By letting $\mathbf{C}_{\mathrm{t}} = \int_{\Gamma_2} \mathbf{N}_{\mathrm{p}}^{\mathrm{T}} \boldsymbol{\Phi}_0 \mathrm{d}\Gamma_2$, the combination of Eq. (12) and Eq. (52) gives

$$\begin{bmatrix} \mathbf{0} & -\lambda\mathbf{C}_{\mathrm{r2}} & \lambda\mathbf{C}_{\mathrm{t}} & \mathbf{K}(k_x) - \omega^2\mathbf{M} \\ \lambda\mathbf{I} & \mathbf{0} & \mathbf{0} & -\mathrm{i}\omega\mathbf{E}_{\mathrm{r2}} \\ -\lambda\mathbf{G}_{\mathrm{r2}} & \lambda\mathbf{H}_{\mathrm{r2}} & \mathbf{0} & \mathbf{0} \end{bmatrix} \begin{bmatrix} \bar{\mathbf{v}}_{\mathrm{r2n}} \\ \bar{\mathbf{p}}_{\mathrm{r2n}} \\ \bar{\mathbf{p}}_0 \\ \lambda\bar{\mathbf{q}} \end{bmatrix} = \begin{bmatrix} \lambda\left(\bar{\mathbf{F}}_{\mathrm{f}} + \bar{\mathbf{F}}_{\mathrm{s}}\right) \\ \mathbf{0} \\ \mathbf{0} \end{bmatrix}. \tag{53}$$

Combining Eqs. (49), (51) and (53) gives

$$\begin{bmatrix} \mathbf{0} & -\lambda\mathbf{C}_{\mathrm{r2}} & \mathbf{0} & \mathbf{0} & \lambda\mathbf{C}_{\mathrm{t}} & \mathbf{K}(k_x) - \omega^2\mathbf{M} \\ \lambda\mathbf{I} & \mathbf{0} & \mathbf{0} & \mathbf{0} & \mathbf{0} & -\mathrm{i}\omega\mathbf{E}_{\mathrm{r2}} \\ -\lambda\mathbf{G}_{\mathrm{r2}} & \lambda\mathbf{H}_{\mathrm{r2}} & \mathbf{0} & \mathbf{0} & \mathbf{0} & \mathbf{0} \\ \mathbf{0} & \mathbf{0} & \lambda\mathbf{A}_{\mathrm{L}}^{-} & \lambda\mathbf{A}_{\mathrm{R}}^{-} & \lambda\mathbf{A}_{0}^{-} & \mathbf{0} \\ \mathbf{0} & \mathbf{0} & \lambda\mathbf{A}_{\mathrm{L}}^{+} & \lambda\mathbf{A}_{\mathrm{R}}^{+} & \lambda\mathbf{A}_{0}^{+} & \mathbf{0} \\ \mathbf{0} & \mathbf{0} & \lambda\mathbf{A}_{\mathrm{L}}^{0} & \lambda\mathbf{A}_{\mathrm{R}}^{0} & \lambda\mathbf{A}_{0}^{0} & -\mathbf{E}_{\mathrm{t}} \end{bmatrix} \begin{bmatrix} \bar{\mathbf{v}}_{\mathrm{r2n}} \\ \bar{\mathbf{p}}_{\mathrm{r2n}} \\ \bar{\mathbf{p}}_{\mathrm{L}} \\ \bar{\mathbf{p}}_{\mathrm{R}} \\ \bar{\mathbf{p}}_0 \\ \lambda\bar{\mathbf{q}} \end{bmatrix} = \begin{bmatrix} \lambda\left(\bar{\mathbf{F}}_{\mathrm{f}} + \bar{\mathbf{F}}_{\mathrm{s}}\right) \\ \mathbf{0} \\ \mathbf{0} \\ \mathbf{0} \\ \mathbf{0} \\ \mathbf{0} \end{bmatrix}, \tag{54}$$

This equation can finally be inverted to determine the vector of responses due to the excitation on the right-hand side for each wavenumber k_x and frequency ω.

2.4 Radiated sound power and STL

The nodal tractions $\bar{\mathbf{p}}_{\mathrm{L}}$, $\bar{\mathbf{p}}_{\mathrm{R}}$ and $\bar{\mathbf{p}}_0$, determined by Eq. (54), can be used to calculate the Fourier-transformed traction $\tilde{\boldsymbol{\tau}}(k_x, k_y')$ in the coordinate system *oxyz* by using Eq. (40). From the coordinate system rotation or transformation of Eq. (29), the traction $\tilde{\boldsymbol{\tau}}\left(k_x, k_y'\right)$ in the coordinate system *ox'y'z* can be obtained. Then the equation governing the vibration of the acoustic treatment layer, i.e. Eq. (13), can be used to calculate the sound pressure $\tilde{p}_2^{f2}\left(\mathrm{M}_{\mathrm{f2}}\right)$ and normal velocity $\tilde{v}_2^{f2}\left(\mathrm{M}_{\mathrm{f2}}\right)$ in Fluid 2 at the interface with the acoustic treatment layer.

The sound power radiated by the acoustically treated panel into Fluid 2 can be calculated as

$$W_{\mathrm{rad}} = \frac{1}{8\pi^2} \mathrm{Re} \int_{-\infty}^{+\infty} \int_{-\infty}^{+\infty} \tilde{p}_2^{f2}\left(\mathrm{M}_{\mathrm{f2}}\right) \tilde{v}_2^{f2}\left(\mathrm{M}_{\mathrm{f2}}\right)^{*} \mathrm{d}k_x \mathrm{d}k_y' , \tag{55}$$

where * denotes complex conjugate. For the incident plane wave with incident angles φ and ψ, as shown in Fig. 4, the incident sound power per unit length in the *x*-direction can be calculated as [35]

$$W_{\text{inc}} = \frac{\left|\bar{p}_{\text{i}}\right|^2 l_y \cos\theta}{2\rho_1 c_1}, \tag{56}$$

where $l_y = 2b$ is the width of the base panel; ρ_1 and c_1 are, respectively, the density and sound speed of Fluid 1. The transmitted sound power per unit length in the x-direction can be calculated as

$$W_{\text{trans}} = \frac{1}{4\pi}\text{Re}\int_{-\infty}^{+\infty} \bar{p}^{f2}\left(\text{M}_{\text{f2}}\right)\bar{v}_2^{f2}\left(\text{M}_{\text{f2}}\right)^* \text{d}k_y' . \tag{57}$$

The ratio of the incident sound power to the transmitted sound power gives the sound power transmission coefficient τ which is used to calculate the sound transmission loss of the acoustically treated panel, i.e.

$$\tau = \frac{W_{\text{trans}}}{W_{\text{inc}}}, \tag{58}$$

$$\text{STL} = 10\log_{10}\left(\frac{1}{\tau}\right). \tag{59}$$

The diffuse field sound transmission loss can be calculated as

$$\text{STL}_{\text{d}} = 10\log_{10}\left(\frac{1}{\tau_{\text{d}}}\right), \tag{60}$$

where τ_{d} is the diffuse field sound power transmission coefficient, i.e.

$$\tau_{\text{d}} = \frac{\int_{\psi_{\text{lim}}}^{\pi/2}\int_{\varphi_{\text{lim}}}^{\pi/2}\tau\left(\psi,\varphi\right)\sin^2\psi\sin\varphi\,\text{d}\varphi\,\text{d}\psi}{\int_{\psi_{\text{lim}}}^{\pi/2}\int_{\varphi_{\text{lim}}}^{\pi/2}\sin^2\psi\sin\varphi\,\text{d}\varphi\,\text{d}\psi}, \tag{61}$$

where φ_{lim} and ψ_{lim} are the integral limiting angles, which are usually set to be 12° and 0° for the field incidence and full random incidence, respectively [35, 47].

3. Comparison with other methods

In this section, the model established in Section 2 (termed the 2.5D FEM-BEM-TMM model) is compared with a full 2.5D FE-BE model (which has been developed by the current authors by extending the work presented in Ref. [46]). In the 2.5D FEM-BEM-TMM model, as shown in Fig. 2 and Section 2, the acoustic treatment layer is assumed to consist of a number of homogeneous layers of infinite width and length, but the base panel has a finite width, whereas in practice the acoustic treatment layer has the same width as the base panel. The base panel plus Fluid 1 is dealt with using the 2.5D FE-BE method, and the acoustic treatment layer plus Fluid 2 is modelled with

TMM, in which the porous layer is modelled based on Biot's theory [43, 44]. In contrast, as shown in Fig. 5, in the full 2.5D FE-BE model both the base panel and the acoustic treatment layer have a finite width, and the 2.5D FE is used to calculate the vibration of the panel and the layers while the 2.5D BE is applied to evaluate the sound radiation on both sides. The 2.5D FE model for the porous sub-layer is based on an equivalent mixed displacement-pressure formulation for Biot's theory [48]. Thus, the full 2.5D FE-BE model is here termed more clearly the 2.5D FEM-BEM-Biot model. Comparisons in terms of STL are performed by applying the two models to a thin plate (base panel) with an acoustic treatment layer. Results from the 2.5D FEM-BEM-Biot model serve as the benchmark for the other model.

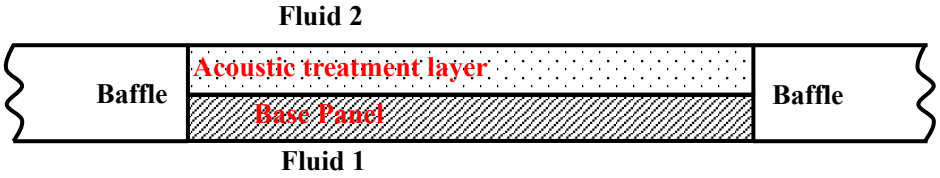

Fig. 5 A Sketch of a baffled panel and a baffled acoustic treatment layer

3.1 Parameters and elements

The base panel is assumed to be made of aluminium alloy with the material properties listed in Tab. 1. The damping loss factor is set to be 0.005, according to Ref. [5]. It has a thickness of 6 mm and a width of either 1000 mm or 2000 mm. At the two side boundaries along the infinitely long direction the base panel is simply supported. The acoustic treatment contains a single layer of either melamine foam or glass wool with a thickness of either 50 mm or 100 mm. The material properties are listed in Tab. 2. The symbols α_∞, ϕ, σ, Λ and Λ' in Tab. 2 are, respectively, the tortuosity, porosity, flow resistivity, viscous characteristic length and thermal characteristic length. The symbols ρ_s, E, υ and η are, respectively, the density, Young's modulus, Poisson's ratio and loss factor of the frame in vacuum. The main difference between the two porous materials lies in that the glass wool is stiffer, heavier and has a larger flow resistivity than the melamine foam. The masses per unit area of the base panel, the melamine foam layer and the glass wool layer are 16.2 kg/m^2, 0.55 kg/m^2 (50 mm in thickness) and 6.5 kg/m^2 (50 mm in thickness). The Young's modulus-to-density ratios (in units Nm/kg) of the three are 2.63×10^7, 1.09×10^4 and 3.38×10^4. It can be seen that, compared to the base panel, the melamine foam layer is light and soft while the glass wool layer is not that light but still soft.

Tab. 1 Material properties of the base panel [5, 33]

Young's modulus (Pa)	Density (kg/m^3)	Poisson's ratio	Loss factor
7.1×10^{10}	2.7×10^{3}	0.332	0.005

Tab. 2 Properties of saturated fluid and frame of the melamine foam [46] and glass wool [48]

Porous material	α_∞	ϕ	σ (Ns/m^4)	Λ (μm)	Λ' (μm)	ρ_s (kg/m^3)	E (Pa)	υ	η
Melamine foam	1.06	0.97	11000	150	200	11	1.2×10^5	0.42	0.15
Glass wool	1.06	0.94	40000	56	110	130	4.4×10^6	0	0.1

For the 2.5D FEM-BEM-TMM model, the base panel is meshed with 3-noded 2.5D shell elements. The size of an element is about 15 mm. The left and right baffles are truncated and discretized with the same mesh size as the base panel. In the lateral direction, the layer of porous material can be divided into three parts: the left porous layer that is supported by the left part of the baffle, the middle porous layer that is in contact with the base panel, and the right porous layer that is supported by the right part of the baffle. For the 2.5D FEM-BEM-Biot model, the acoustic treatment layer is meshed with 8-noded 2.5D solid elements of sizes similar to those for the base panel. The acoustic treatment layer is assumed to be glued to the baffle. The Champoux-Allard-Johnson model [41, 42] for calculating the frequency-dependent parameters of a porous medium is implemented in both the 2.5D FEM-BEM-TMM and 2.5D FEM-BEM-Biot models. Nodes on the air/structure interfaces form the boundary elements required for the sound radiation calculation. In the following Section 3.2 and Section 3.3, the oblique incidence at $\psi = 45^o$ and $\varphi = 45^o$ is considered. The incident sound wave has a non-zero wavenumber in both the longitudinal and lateral directions. The STL is calculated using Eqs. (58) and (59).

3.2 Effect of baffle truncation in the 2.5D FEM-BEM-TMM model

In the 2.5D FEM-BEM-TMM model, conditions on the interface between the baffle and the acoustic treatment layer are satisfied only for a finite width of b^* on both sides. The effect of this treatment (truncation) is now investigated and results are shown in Fig. 6 for b^* = 100, 500, 1000 and 2000 mm. Aparrent differences occur at low frequencies but the results converge at high frequencies. This may be explained by the fact that the vibration of the acoustic treatment layer decays more slowly along the lateral direction at low frequencies than at high frequencies [45]. Therefore, to calculate STL at low frequencies a larger b^* is required.

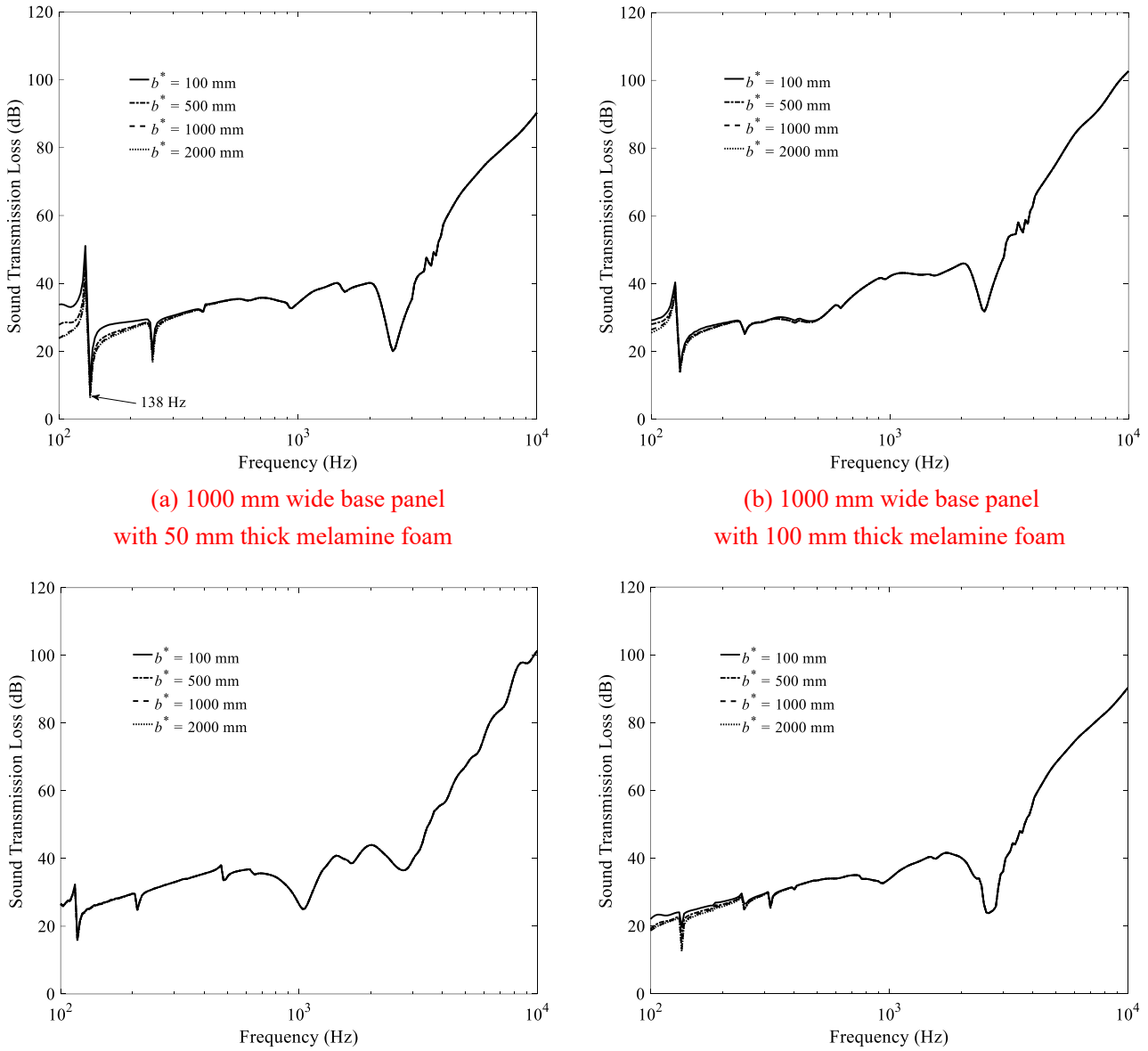

(a) 1000 mm wide base panel with 50 mm thick melamine foam

(b) 1000 mm wide base panel with 100 mm thick melamine foam

(c) 1000 mm wide base panel with 50 mm thick glass wool

(d) 2000 mm wide base panel with 50 mm thick melamine foam

Fig. 6 Effect of baffle/acoustic treatment layer interface truncation on the STL predicted by the 2.5D FEM-BEM-TMM model for incident angles $\psi = 45^o$ and $\varphi = 45^o$

It can also be seen from Fig. 6 that the required width depends on the width of the base panel, the applied porous material and the thickness of the porous layer. For the 1000 mm wide base panel with a 50 mm-layer of melamine foam (Fig. 6(a)), b^* can be taken as 1000 mm, while for the same base panel with a 50 mm-layer of glass wool (Fig. 6(c)), b^* can be reduced to less than 100 mm. This may be explained by the larger flow resistivity of the glass wool. As the viscous damping of the porous material increases with increasing thickness, a porous layer with a larger thickness allows the STL to converge more rapidly with increasing of b^*. This is demonstrated by a comparison of Fig. 6(a) with a 50 mm-layer of melamine foam and Fig. 6(b) with a 100 mm-layer of melamine foam.

A significant effect of truncation can be found in Fig. 6(a) below about 138 Hz, at which the second lateral mode of the base panel cuts on. Since a wide base panel causes lateral modes to shift towards low frequencies, the required value of b^* decreases to about 500 mm for the 2000 mm wide base panel (Fig. 6(d)) compared with 1000 mm in Fig. 6(a). It is difficult to derive a general rule to determine b^*, and therefore for a given panel and acoustic treatment, trials should be performed to determine the appropriate sizes of elements and truncation.

3.3 Comparison of STL between the two methods

The STLs predicted using the two methods are compared in Fig. 7. According to the results in Section 3.2, b^* is taken to be 1000 mm in the 2.5D FEM-BEM-TMM model. It can be seen from each figure in Fig. 7 that, above a certain frequency, the two models give almost the same result. This is about 900 Hz in Fig. 7(a), 1100 Hz in Fig. 7(b), 1000 Hz in Fig. 7(c) and 700 Hz in Fig. 7(d), depending on the width of the base panel, the material properties and thickness of the porous layer. The agreement between the two models at high frequencies may be attributed to the fact that the transmitted sound power in the 2.5D FEM-BEM-TMM model becomes dominated by the middle region of the surface of the porous layer, and is almost unaffected by the region beyond the panel. The difference at about 1570 Hz in Fig. 7(a), 1534 Hz in Fig. 7(b), 1607 Hz in Fig. 7(c) and 1570 Hz in Fig. 7(d) is due to the cut-on of a propagating wave in the base panel.

Apparent differences up to 4 dB between the two models can be seen at lower frequencies. Here, the 2.5D FEM-BEM-TMM model predicts higher STLs than the 2.5D FEM-BEM-Biot model. This may be explained by the larger absorbing area introduced by the left and right porous layers in the TMM and the restraint of the porous layer vibration due to the rigid attachment to the left and right baffles.

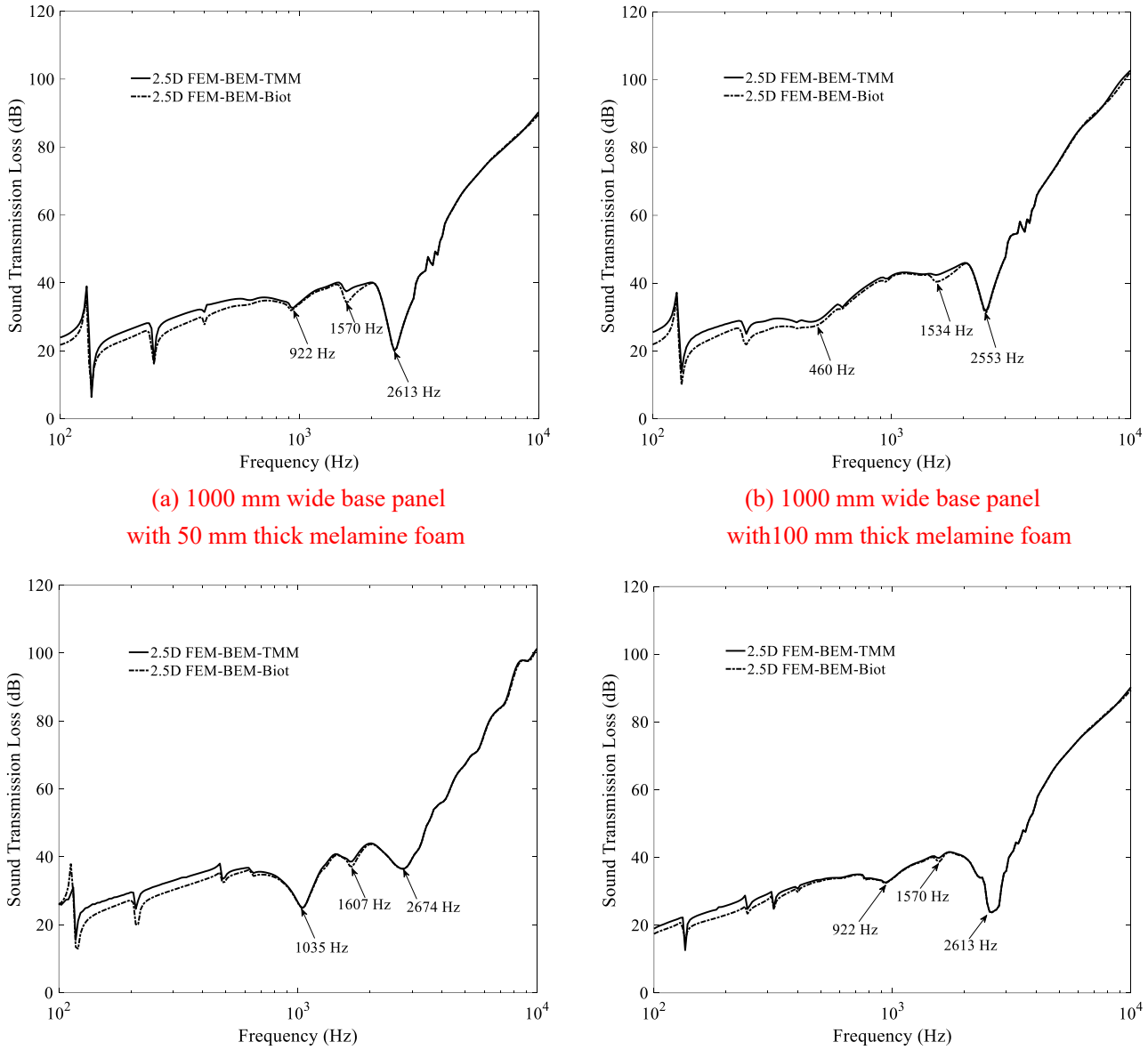

(a) 1000 mm wide base panel with 50 mm thick melamine foam

(b) 1000 mm wide base panel with100 mm thick melamine foam

(c) 1000 mm wide base panel with 50 mm thick glass wool

(d) 2000 mm wide base panel with 50 mm thick melamine foam

Fig. 7 Comparison in STL predicted using 2.5D FEM-BEM-TMM and 2.5D FEM-BEM-Biot for incident angles $\psi = 45^{\circ}$ and $\varphi = 45^{\circ}$

Figure 7(a), Fig. 7(b) and Fig. 7(c) show a dip at around 922 Hz, 460 Hz, and 1035 Hz, respectively. This dip is caused by the resonance of the frame of the porous material on the base panel. The resonance frequency can be determined by the fact that, at this frequency, the compressional wavelength in the thickness direction of the frame is equal to four times the thickness (h) of the porous layer, i.e. [45]

$$f_{\mathrm{r}} = \frac{1}{4h} \Bigg/ \sqrt{\frac{\rho_{\mathrm{s}}}{K_{\mathrm{c}}} - \frac{1}{c_1^2}\sin^2\theta}\,, \tag{62}$$

where $\theta = \arccos\left(\sin\psi \sin\varphi\right)$ is the incident angle (Fig. 4), c_1 is the sound speed of Fluid 1, and

$$K_c = \frac{(1-\upsilon)E}{(1+\upsilon)(1-2\upsilon)}. \tag{63}$$

With the elastic parameters of the melamine foam and the glass wool listed in Tab. 2, Eq. (62) gives 919 Hz, 459 Hz and 1038 Hz, which are almost identical to the frequencies observed in the figures. Since the thickness of the melamine foam in Fig. 7(d) is identical to that in Fig. 7(a), the same resonance frequency 922 Hz is predicted in Fig. 7(d).

There is a deep dip at around 2613 Hz in Fig. 7(a), 2553 Hz in Fig. 7(b), 2674 Hz in Fig. 7(c) and 2613 Hz in Fig. 7(d). These frequencies are the coincidence frequencies (at which the acoustic wavenumber in the longitudinal direction is identical to the structural wavenumber in the same direction) of the composite structure. The coincidence frequency is mainly determined by the bending stiffness and mass per unit area of the base panel. The acoustic treatments have small effect on these two quantities and consequently, the coincidence frequencies shown in Fig. 7 are similar to each other.

3.4 Comparison of computational efficiency between the two methods

The computation time required to calculate the STL using the two models for a single incident angle and with 200 log-spaced frequencies from 100 Hz to 10000 Hz are compared in Tab. 3. The predictions were conducted using a PC with 16 GB memory and 3.2 GHz dual core processor. The 2.5D FEM-BEM-TMM model established in this paper is about three times faster than the 2.5D FEM-BEM-Biot model. It can be expected that the advantages in computation time become much more significant for an acoustic treatment consisting of many thin sub-layers.

Tab. 3 Comparison in computation time between the two methods

Method	2.5D FEM-BEM-TMM	2.5D FEM-BEM-Biot
Computation time (seconds)	600	1800

In summary, for a panel consisting of homogeneous layers, it is demonstrated that the 2.5D FEM-BEM-TMM can give results matching well with the 2.5D FEM-BEM-Biot model with a much-reduced computation time, especially for high frequencies. Therefore, in the next section, the 2.5D FEM-BEM-TMM is applied to predict the STL for a typical rib-stiffened panel from a train carriage, acoustically treated with different porous material layers.

4. Application to an acoustically treated rib-stiffened panel from a train carriage

The vibro-acoustic behaviour of the floor structure of a train has a great effect on the interior noise of the train. The floor consists of a rib-stiffened panel, layers of porous materials and a wooden floor. The vibro-acoustic behaviour of the floor structure is investigated in this section using the 2.5D FEM-BEM-TMM model proposed in Section 2. The presence of the wooden floor will be neglected, since the aim of this paper is to investigate the effect of the acoustic treatment layer on the STL of the base panel. The width of the panel is reduced to have a size similar to that in standard STL measurement.

4.1 Parameters and elements

As shown in Fig. 8, the base panel is a double-leaf panel stiffened by truss-core stiffeners. The thickness of the base panel is 50 mm, its width is 970 mm, similar to the widths of samples used for STL measurements [36]. The thicknesses of the bottom and top face panels and the intermediate stiffeners are 4.2 mm, 4.15 mm and 2.43 mm, respectively. The material properties of the base panel are the same as those of the thin plate in Section 3. The top and bottom face panels are simply supported along their side boundaries, as shown in Fig. 9. The panel is meshed with 2.5D 3-noded shell elements with a maximum size of 30 mm.

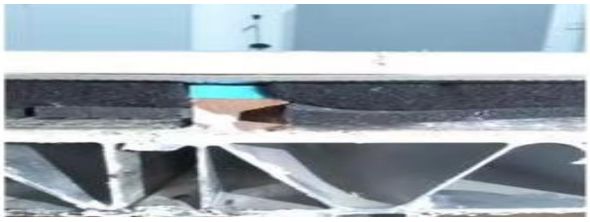

Fig. 8 A train floor structure

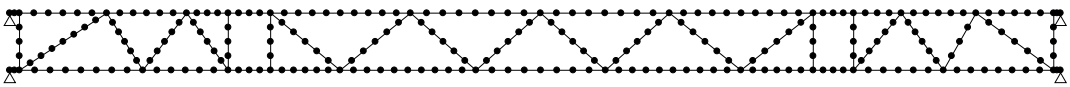

Fig. 9 Mesh and boundary condition of the rib-stiffened panel

The acoustic treatment layer can be formed of a single layer of porous material or multiple sub-layers of different porous materials. The thickness of the acoustic treatment layer is set to be 60 mm, similar to that found on typical high-speed trains. A number of configurations are considered based on the materials listed in Tab. 2.

4.2 Sound absorption coefficient of the acoustic treatment layer

The normal incidence sound absorption coefficients of four different acoustic treatment configurations are predicted using TMM with the bottom surface fixed. The predicted absorption coefficients are shown in Fig. 10. The four configurations are: a single layer of melamine foam, a single layer of glass wool and two sub-layers of the two materials arranged in either order. For the latter two configurations, both sub-layers have the same thickness.

Due to the large differences in flow resistivity, density and Young's modulus between the porous materials, sound absorptions of the four acoustic treatment configurations are quite different from each other at frequencies below about 2000 Hz, and all change rapidly with frequency. However, above about 3000 Hz (the acoustic wavelength is shorter than 114 mm), the differences become much reduced and the absorption coefficients are all close to 1, due to the similar porosities of the two porous materials.

It can be seen that below about 1000 Hz, the 60 mm-layer of glass wool has higher absorption than the 60 mm-layer of melamine foam, but for frequencies between about 1000 Hz and 2000 Hz, the latter is more sound-absorbent than the former. On the other hand, the 'base-glass wool-melamine foam' configuration is the best (in terms of normal incidence sound absorption coefficient) of the four configurations for frequencies higher than about 1500 Hz. The absorption of the two-layer treatment is similar to that of a single layer of the material of the upper layer especially at lower frequencies.

A dip absorption coefficient occurs at around 660 Hz for the 60 mm-layer of melamine foam and 690 Hz for the 60 mm-layer of glass wool. This is due to the resonance of the material frame. Eq. (62) gives the resonance frequency for normal incidence at about 695 Hz and 766 Hz, which are a little higher than the observed ones. A dip occurs at about 230 Hz for the 'base-melamine foam-glass wool' configuration. This is caused by the resonance of a spring-mass system, in which the bottom layer acts as a spring and the outer layer as a mass. For the 'base-glass wool-melamine foam' configuration, there is a dip at 1090 Hz due mainly to standing waves in the outer melamine foam layer. Other dips at higher frequencies are caused by standing waves in the saturated fluid.

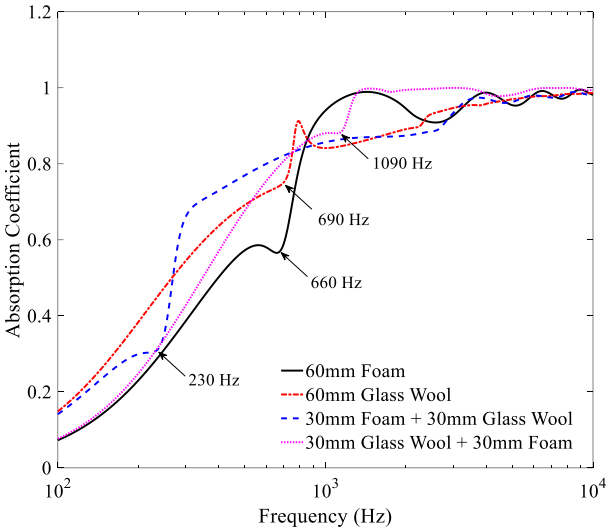

Fig. 10 The normal incidence sound absorption coefficients of the four acoustic treatment layer configurations

4.3 Influence of acoustic treatment layer configuration on the diffuse field STL

The diffuse field STL of the rib-stiffened base panel (Fig. 9) with or without the above acoustic treatment is predicted and shown in Fig. 11. The diffuse field STL is calculated using Eqs. (60) and (61). Here, the full random incidence with φ_{lim} and ψ_{lim} in Eq. (61) both set to be 0º is considered with an integral step of 8º for the diffuse field STL prediction. The angle increment has been chosen considering both prediction accuracy and computation time. Although it has been demonstrated in Section 3 that the results below 630 Hz differ from those of the 2.5D FEM-BEM-Biot model, results are still shown at lower frequencies as the relative differences between treatments are still of interest.

There are significant differences between the results for the different layer configurations, with a range of almost 10 dB above 630 Hz. In this frequency range even the single layer of melamine foam, which gives the lowest STL, gives an improvement of 5-10 dB over that of the bare panel. The single layer of glass wool produces a greater STL than the single layer of melamine foam, since the glass wool has a higher flow resistivity, which significantly affects the dissipation mechanism, and is heavier than the melamine foam, also beneficial to STL. The two-layer acoustic treatment with a first sub-layer of melamine foam has the highest STL, whereas the one with the glass wool as the first sub-layer has a similar STL to that containing a single layer of melamine foam. Below 630 Hz, the differences are more modest and should be treated with caution due to the fact the vibration decaying rate, in the lateral (infinite) direction, depends on the acoustic treatment configurations discussed in Section 3.3.

The dip occurring at 250 Hz for the base panel is caused by its first lateral mode. This dip

shifts to 200 Hz for the base panel with a single layer of glass wool, due to the additional mass of the glass wool. For the single layer of melamine foam, since the added mass is much smaller than for the glass wool, this dip stays at 250 Hz. For the two-layer treatment with the melamine foam nearest to the panel, the dip at 200 Hz corresponds to the resonance of a mass-spring-mass system, in which the base panel and glass wool layer act as the masses and the foam layer forms the spring. A similar feature was seen as a dip in the absorption coefficient in Fig. 10. It is due to this resonance that this treatment has the highest STL at higher frequencies (the glass wool is largely isolated by the melamine foam from the vibration of the base panel).

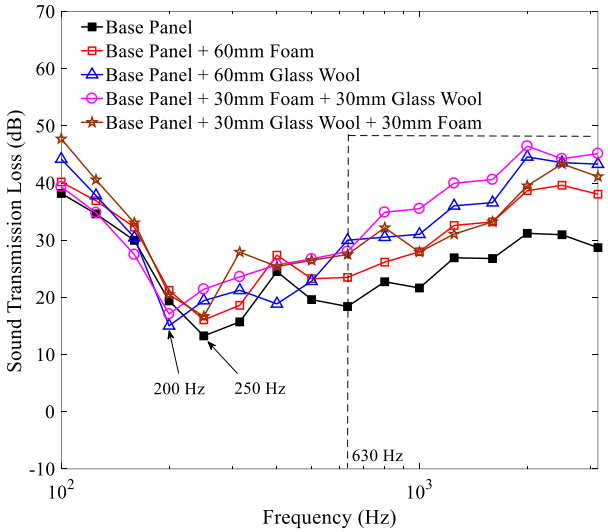

Fig. 11 Influence of the acoustic treatment layer configuration on the diffuse field STL of the rib-stiffened panel

To illustrate the reasons for these differences and the dips, results are determined using the same combinations of porous layers attached to the thin plate in Section 3. The normal incidence STL predicted using TMM is shown in Fig. 12. The dips above around 1500 Hz for the four configurations are due to the standing waves of the saturated fluid, especially in the glass wool. The treatments all give an improvement to the STL at high frequency but it is reduced at low frequency, especially around the main dip. This dip occurs at around 580 Hz for the single layer of glass wool and 682 Hz for the single layer of foam. This is caused by the resonance of the material frame and is similar to the dip seen in the absorption coefficient in Fig. 10. A dip occurs at around 215 Hz for the two-sub layers with the melamine foam nearest the panel which is attributed to the resonance of a mass-spring-mass system. For the two-layer treatment in the other order a dip occurs at 1110 Hz, which is due to the standing waves in the outer foam layer.

The resonance frequency of the mass-spring-mass system, termed the MSM resonance

frequency, can be evaluated by [11]

$$f_{\mathrm{MSM}} = \frac{1}{2\pi\cos\theta}\sqrt{\frac{k'\left(m_{\mathrm{p1}}+m_{\mathrm{p2}}\right)}{m_{\mathrm{p1}}m_{\mathrm{p2}}}}, \tag{64}$$

where m_{p1} and m_{p2} are the mass per unit area of the two outer layers; θ is the incident angle; k' is the equivalent stiffness of the middle layer, which can be approximately calculated as

$$k' = \frac{K'_{\mathrm{c}}}{h}. \tag{65}$$

In Eq. (65), h is the thickness of the middle layer and K'_{c} is the elastic constant of the compressional wave of the middle layer. As the fluid is effectively trapped in the foam layer by the higher flow resistivity of the outer glass wool layer, the modulus K'_{c} should include the effect of compressibility of the fluid. It can be approximately evaluated by

$$K'_{\mathrm{c}} = \left(1-\phi\right)K_{\mathrm{c}}^{\mathrm{s}} + \phi K_{\mathrm{c}}^{\mathrm{f}}, \tag{66}$$

where $K_{\mathrm{c}}^{\mathrm{s}}$ and $K_{\mathrm{c}}^{\mathrm{f}}$ are the elastic constants of the frame and the fluid, respectively. Thus, with the properties listed Tab. 2, Eqs. (64), (65) and (66) give the MSM resonance frequency at around 205 Hz, which is close to the dip frequency observed in the figure. This value would be 50 Hz if the effect of compressibility of the fluid is neglected. It is worth noting that Eq. (64) reduces to the resonance frequency of the spring-mass system presented in Section 4.2 if $m_{p1} \to \infty$. Below the MSM resonance frequency both masses move together but above it they are isolated by the spring. This leads to the rapidly rising STL above the MSM resonance frequency.

Therefore, returning to Fig. 11 for the acoustically treated rib-stiffened panel, it is reasonable that the acoustic treatment with a first sub-layer of melamine foam gives the highest STL across the frequency range considered, while that with a first sub-layer of glass wool gives results that are comparable with or even worse than those for a single layer of foam.

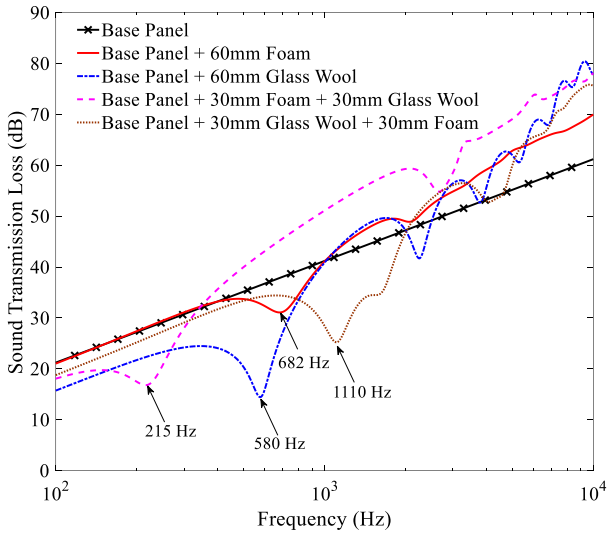

Fig. 12 Influence of the acoustic treatment layer configuration on normal incidence STL of a thin plate predicted using TMM

Considering the absorption coefficients in Fig. 10, it is clear that a higher absorption coefficient does not necessarily mean a better STL of the acoustically treated panel. For example, the 60 mm-layer of melamine foam has a higher absorption between 1000 Hz and 2000 Hz, but performs less well than the 60 mm-layer of glass wool; below 1000 Hz, the results in Fig. 12 indicate that glass wool has a lower STL where it has a higher absorption coefficient. This is because that the absorption coefficient is obtained by fixing the back face of the porous material layer, while the back face vibrates together with the base panel in operation and the vibration of the frame can also radiate sound into the acoustic domain.

4.4 Influence of the thickness ratio of the two sub-layers

As previously demonstrated, the two-layered acoustic treatment formed of the melamine foam as the first sub-layer gives a higher STL than other configurations. The influence of the thickness ratio of the melamine foam to the glass wool on the STL are investigated here with the total thickness kept to be 60 mm. Results are shown in Fig. 13(a) for thickness ratios of 10/50, 20/40, 30/30, 40/20 and 50/10. The MSM resonance dip frequencies of the five cases are 190 Hz, 195 Hz, 196 Hz, 200 Hz and 210 Hz, which are obtained from narrow bands results. The case with the thickness ratio of 10/50, i.e. 10 mm melamine foam and 50 mm glass wool, has the resonance dip at the lowest frequency and consequently the highest STL above 630 Hz. Fig. 13(b) shows the average improvement in STL relative to the base panel for the frequency bands above 630 Hz. This confirms that the acoustic treatment configuration of two sub-layers with the thickness ratio of 10/50 has the best performance.

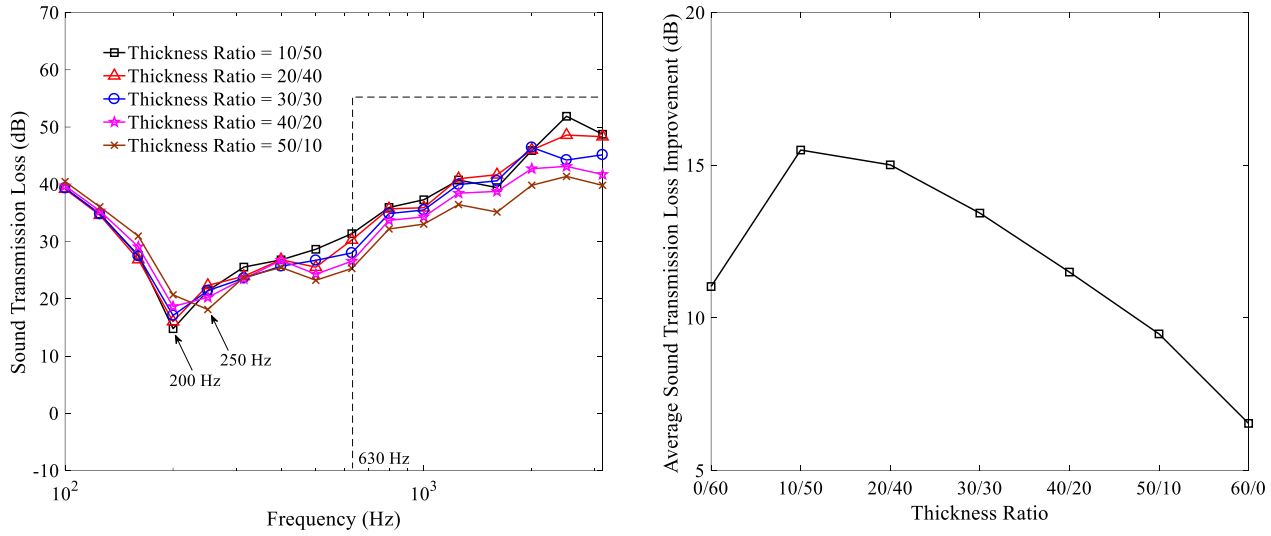

(a) Diffuse field STL (b) Average STL improvement above 630 Hz

Fig. 13 Influence of the thickness ratio of the two-layered acoustic treatment with the foam as the first sub-layer on STL

5. Conclusions

In this paper, a relatively efficient method (2.5D FEM-BEM-TMM) is proposed to study the vibro-acoustic behaviour of complex rib-stiffened panels with multiple layers of acoustic treatment. According to the method, the 2.5D structural finite element method, the 2.5D acoustical boundary element method and the transfer matrix method are combined to perform the prediction. The accuracy of the method is demonstrated by applying it to a homogeneous thin plate with an acoustic treatment and comparing it with the full 2.5D FE-BE method (the 2.5D FE-BE-Biot model). The method is applied to study the effect of different acoustic treatments on the STL of a rib-stiffened panel commonly used in train carriages.

The 2.5D FE-BE-TMM method established in this paper can reduce computation times, by about a factor of three for a single porous layer, compared with the full 2.5D FE-BE-Biot method. The two methods predict similar results above a certain frequency, which depends on the configuration. Below this frequency differences exist because the TMM requires the porous treatment to be extended over the adjacent baffle.

The layer configuration of the acoustic treatment greatly affects the STL, giving improvements of 5-15 dB compared with the bare panel. It is recommended that the first sub-layer of the acoustic treatment should be formed of a soft porous material with a heavier upper layer to obtain a relatively high STL. This effect can be explained in terms of the introduction of a mass-spring-mass resonance.

Acknowledgements

This work was supported by the Ministry of Science and Technology of China (2016YFE0205200).

References

[1] D. J. Thompson, Railway Noise and Vibration, Mechanism, modelling and means of control, first ed., Elsevier Science, 2009.

[2] U. Orrenius, Transmission of Structure-Borne Sound in Ships: Applications to a Prediction Model, PhD thesis, KTH, 1997.

[3] U. Orrenius, Analysis of sound transmission through aircraft fuselages excited by turbulent boundary layer or diffuse acoustic pressure fields, Proc. of Inter-Noise, 2009.

[4] G. Xie, D.J. Thompson, C.J.C. Jones, A modelling approach for the vibroacoustic behaviour of aluminium extrusions used in railway vehicles. J. Sound Vib. 293 (2006) 921-932.

[5] Y. Zhang, D.J. Thompson, G. Squicciarini, J. Ryue, X. Xiao, Sound transmission loss properties of truss core extruded panels, Appl. Acoust. 131 (2018) 134-153.

[6] H. Qian, Z. He, W. Jiang, W. Peng, Sound transmission of periodic composite structure lined with porous core: Rib-stiffened double panel case, J. Sound Vib. 440 (2019) 256-276.

[7] C.M. Nilsson, A.N. Thite, C.J.C. Jones, D.J. Thompson, Estimation of sound transmission through extruded panels using a coupled waveguide finite element-boundary element method, in: B. Schulte-Werning, et al. (Eds.) Proceedings of 9th International Workshop on Railway Noise, Munich, Germany, 4-8 September 2007, Notes on Numerical Fluid Mechanics & Multidisciplinary Design 99 (2008) 306-212.

[8] T. Fu, Z. Chen, H. Yu, Z. Wang, X. Liu, An analytical study of sound transmission through corrugated core FGM sandwich plates filled with porous material, Compos: Part B 151 (2018) 161-172.

[9] J. H. Lee, J. Kim, Analysis of sound transmission through periodically stiffened panels by space-harmonic expansion method, J. Sound Vib. 251(2) (2002) 349-366.

[10] J.H. Lee , J. Kim, Sound transmission through periodically stiffened cylindrical shells, J. Sound Vib. 251(3) (2002) 431-456.

[11] J. Wang, T. Lu, J. Woodhouse, R.S. Langley, J. Evans, Sound transmission through lightweight double-leaf partitions: theoretical modelling, J. Sound Vib. 286(4-5) (2005) 817-847.

[12] S. Zhang, X. Sheng, Analysis of sound transmission loss of a rectangular plate with acoustic treatments, Proceedings of ISMA2018 and USD 2018. Brussels: Department of Mechanical Engineering (2018) 725-740.

[13] R. Talebitooti, M.R. Zarastvand, The effect of nature of porous material on diffuse field

acoustic transmission of the sandwich aerospace composite doubly curved shell, Aerosp. Sci. Technol. 78 (2018) 157-170.

[14] R. Talebitooti, M.R. Zarastvand, H.D. Gohari, The influence of boundaries on sound insulation of the multilayered aerospace poroelastic composite structure, Aerosp. Sci. Technol. 80 (2018) 452-471.

[15] F. Xin, T. Lu, Sound radiation of orthogonally rib-stiffened sandwich structures with cavity absorption, Composites Science and Technology 70 (2010) 2198-2206.

[16] D. Wang, M. Li, Z. Wen, Sound transmission through a sandwich structure with two layered pyramidal core and cavity absorption, J. Sound Vib. 459 (2019) 114853.

[17] O.C. Zienkiewicz, R.L. Taylor, The Finite Element Method, Basic Concepts and linear Applications, 3rd ed., McGraw Hill, 1989.

[18] G. Xie, D.J. Thompson, C.J.C. Jones, Mode count and modal density of structural systems: relationships with boundary conditions, J. Sound Vib. 274 (2004) 621-651.

[19] R.H. Lyon, R.G. DeJong, Theory and Application of Statistical Energy Analysis, 2nd ed., Butterworth-Heinemann, 1995.

[20] R.S. Langley, P. Bremner, A hybrid method for the vibration analysis of complex structural-acoustic systems, J. Acoust. Soc. Am. 105 (3) (1999) 1657-1671.

[21] P.J. Shorter, R.S. Langley, Vibro-acoustic analysis of complex systems, J. Sound Vib. 288 (2005) 669-699.

[22] V. Cotoni, P. Shorter, R. Langley, Numerical and experimental validation of a hybrid finite element-statistical energy analysis method, J. Acoust. Soc. Am. 122 (1) (2007) 259-270.

[23] B.R. Mace, D. Duhamel, M.J. Brennan, L. Hinke, Finite element prediction of wave motion in structural waveguides, J. Acoust. Soc. Am. 117 (2005) 2835-2843.

[24] B.R. Mace, E. Manconi, Modelling wave propagation in two-dimensional structures using finite element analysis, J. Sound Vib. 318 (2008) 884-902.

[25] U. Orrenius, H. Liu, A. Wareing, S. Finnveden, V. Cotoni, Wave modelling in predictive vibro-acoustics: application to rail vehicles and aircrafts, Wave motion 51 (2014) 635-649.

[26] F. Errico, M. Ichchou, S. De Rosa, O. Bareille, F. Franco, The modelling of the flow-induced vibrations of periodic flat and axial-symmetric structures with a wave-based method, J. Sound Vib. 424 (2018) 32-47.

[27] F. Errico, M. Ichchou, F. Franco, S. De Rosa, O. Bareille, C. Droz, Schemes for the sound

transmission of flat, curved and axisymmetric structures excited by aerodynamic and acoustic sources, J. Sound Vib. 456 (2019) 221-238.

[28] V. Cotoni, R.S. Langley, P.J. Shorter, A statistical energy analysis subsystem formulation using finite element and periodic structure theory, J. Sound Vib. 318 (2008) 1077-1108.

[29] D. Chronopoulus, M. Ichchou, B. Troclet, O. Bereille, Computing the broadband vibroacoustic response of arbitrarily thick layered panels by a wave finite element approach, Appl. Acoust. 77 (2014) 89-98.

[30] U. Orrenius, S. Finnveden, Calculation of wave propagation in rib-stiffened plate structures, J. Sound Vib. 182 (1996) 203-224.

[31] X. Sheng, C.J.C. Jones, D.J. Thompson, Prediction of ground vibration from trains using wavenumber finite and boundary element methods, J. Sound Vib. 293 (2006): 575-586.

[32] J. Ryue, D.J. Thompson, P.R. White, D.R. Thompson, Investigation of propagating waves in railway tracks at high frequencies, J. Sound Vib. 315 (2008) 157-175.

[33] I. Prasetiyo, Investigation of Sound Transmission in Lightweight Structures Using a waveguide Finite Element/Boundary Element Approach, PhD thesis, University of Southampton, 2012.

[34] M. Villot, C. Guigou, L. Gagliardini, Predicting the acoustical radiation of finite size multi-layered structures by applying spatial windowing of infinite structures, J. Sound Vib. 245 (3) (2001) 433-455.

[35] H. Kim, J. Ryue, D.J. Thompson, A.D. Müller, Application of a wavenumber domain numerical method to the prediction of the radiation efficiency and sound transmission of complex extruded panels, J. Sound Vib. 449 (2019) 98-120.

[36] J. Zhang, X. Xiao, X. Sheng, C. Zhang, R. Wang, X. Jing, SEA and contribution analysis for interior noise of a high speed train, Appl. Acoust. 112 (2016) 158-170.

[37] C.M. Nilsson, J. Ryue, C.J.C. Jones, Theory manual for WANDS 2.1 wavenumber domain FE-BE software for structures and fluids, University of Southampton, 2010.

[38] X. Sheng, T. Zhong, Y. Li, Vibration and sound radiation of slab high-speed railway tracks subject to a moving harmonic load, J. Sound Vib. 395 (2017) 160-186.

[39] M.E. Delany, E.N. Bazley, Acoustical properties of fibrous materials, Appl. Acoust. 3 (1970) 105-116.

[40] I.P. Dunn, W.A. Davern, Calculation of acoustic impedance of multilayer absorbers, Appl. Acoust. 19 (1986) 321-334.

[41] D.L. Johnson, J. Koplik, R. Dashen, Theory of dynamic permeability and tortuosity in fluid-saturated media, J. Fluid Mech. 176 (1987) 379-402.

[42] Y. Champoux, J.F. Allard, Dynamic tortuosity and bulk modulus in air-saturated porous media, J. Appl. Physics 70 (1991) 1975-1979.

[43] M.A. Biot, Theory of propagation of elastic waves in a fluid-saturated porous media. I. Low-frequency range, J. Acoust. Soc. Am. 28(2) (1956) 168-178.

[44] M.A. Biot, Theory of propagation of elastic waves in a fluid-saturated porous media. II. High-frequency range, J. Acoust. Soc. Am. 28(2) (1956) 179-191.

[45] J.F. Allard, N. Atalla, Propagation of sound in porous media, second ed., Wiley, 2009.

[46] H. Jeong, A numerical investigation of noise mitigation for railway track, PhD thesis, University of Southampton, 2018.

[47] L. Beranek, Noise and Vibration Control, McGraw-Hill, 1971.

[48] N. Atalla, R. Paneton, P. Debergue, A mixed displacements-pressure formulation for poroelastic materials, J. Acoust. Soc. Am. 104(3) (1998) 1444-1452.